

Warsaw University of Technology

FACULTY OF
POWER AND AERONAUTICAL ENGINEERING



Master's diploma thesis

in the field of Robotics and Automatic Control

**Enhancing Car-Like Robots' Suspension Systems
to Improve Performance and Load Safety
With Support of Machine Learning**

Yağız Söylegüzel

student record book number 336074

thesis supervisor

Prof. Elżbieta Jarząbowska

Warsaw, 2025

Summary in English

Car-like robots operating in diverse terrains face significant challenges in maintaining load safety and operational performance due to the limitations of traditional suspension control methods. This thesis presents a novel machine learning based framework for active suspension systems specifically designed for car-like robotic platforms, addressing the unique requirements of payload protection and terrain adaptability.

Research develops a comprehensive approach that incorporates an enhanced non-linear quarter-car model that includes realistic effects such as hysteretic friction, adaptive damping coefficients, progressive spring behavior, load variation dynamics, and speed-dependent tire characteristics. Road profiles are generated according to ISO 8608 standards for five road classes (Class A to Class E), enabling comprehensive evaluation across surface conditions from excellent to very poor.

The experimental validation compares our proposed TD3-based controller, passive suspension, LQR, and PID regulators in 20 test cases, spanning four velocities and five road classes. Performance analysis encompasses a few indicators, including root mean square (RMS) body acceleration for comfort analysis, maximum suspension travel for safety validation, and efficiency analysis.

The results show considerable performance improvements, where the TD3 controller achieves a maximum 64% reduction in RMS body acceleration compared to passive systems, and a 42% average improvement in all road classes. The superiority of the machine learning technique is most apparent in challenging terrains where in-use variations in performance are greatest. In challenging road contact conditions (Class D and E), where it is difficult for conventional controllers to deal with the complex nonlinear dynamics, TD3 achieves substantial gains over LQR controllers in 14% better RMS acceleration performance as well as considerably better total control effectiveness.

Keywords: reinforcement learning, active suspension control, TD3 (Twin Delayed DDPG), safety-constrained learning, curriculum learning, vehicle dynamics, car-like robots, ISO 8608, energy efficiency, nonlinear control, LQR control

Streszczenie w języku polskim

Roboty kołowe typu samochodowego działające w zróżnicowanych warunkach terenowych napotykają istotne trudności w utrzymaniu bezpieczeństwa ładunku oraz wysokiej wydajności pracy z powodu ograniczeń tradycyjnych metod sterowania zawieszeniem. Niniejsza praca prezentuje nowatorskie podejście oparte na uczeniu maszynowym dla aktywnych układów zawieszenia, zaprojektowanych specjalnie dla platform robotycznych typu samochodowego, z uwzględnieniem specyficznych wymagań dotyczących ochrony ładunku i adaptacji do nawierzchni.

Badania obejmują kompleksowe podejście z wykorzystaniem rozszerzonego nieliniowego modelu ćwierćpojazdu, który uwzględnia realistyczne efekty takie jak tarcie histerezowe, adaptacyjne współczynniki tłumienia, progresywną charakterystykę sprężyn, dynamikę zmian obciążenia oraz zależne od prędkości właściwości opon. Profile dróg zostały wygenerowane zgodnie z normą ISO 8608 dla pięciu klas nawierzchni (od klasy A do klasy E), co umożliwia pełną ocenę w warunkach od bardzo dobrych do bardzo złych.

Walidacja eksperymentalna porównuje zaproponowany regulator oparty na algorytmie TD3 z zawieszeniem pasywnym oraz regulatorami LQR i PID w 20 scenariuszach testowych, obejmujących cztery prędkości i pięć klas nawierzchni. Analiza wyników uwzględnia kilka wskaźników, w tym średniokwadratowe przyspieszenie nadwozia (RMS) jako miarę komfortu, maksymalne ugięcie zawieszenia jako kryterium bezpieczeństwa oraz analizę efektywności.

Wyniki pokazują znaczną poprawę osiągów: regulator TD3 uzyskał maksymalnie 64% redukcję RMS przyspieszenia nadwozia w porównaniu z systemami pasywnymi oraz średnio 42% poprawę we wszystkich klasach nawierzchni. Wyższość techniki opartej na uczeniu maszynowym jest szczególnie widoczna w trudnych warunkach terenowych, gdzie zmienność osiągów w eksploatacji jest największa. W wymagających warunkach kontaktu z nawierzchnią (klasy D i E), w których konwencjonalne regulatory mają trudności z obsługą złożonej nieliniowej dynamiki, regulator TD3 uzyskał znaczące korzyści w postaci 14% lepszej wartości RMS przyspieszenia w stosunku do regulatora LQR oraz wyraźnie wyższej ogólnej skuteczności sterowania.

Słowa kluczowe: uczenie ze wzmacnieniem, aktywne sterowanie zawieszeniem, TD3 (Twin Delayed DDPG), uczenie z ograniczeniami bezpieczeństwa, uczenie z programem nauczania, dynamika pojazdu, roboty typu samochodowego, ISO 8608, efektywność energetyczna, sterowanie nieliniowe, regulator LQR

Contents

1	Introduction	1
1.1	Background and Motivation	1
1.1.1	Limitations of Traditional Control Methods	2
1.1.2	Computational Efficiency vs. Performance Trade	2
1.1.3	Safety and Constraint Handling	2
1.2	Research Objectives	2
1.2.1	Primary Objective	2
1.2.2	Specific Objectives	3
1.3	Contributions	3
1.3.1	Theoretical Contributions	3
1.3.2	Practical Contributions	3
1.4	Thesis Organization	3
2	Literature Review	4
2.1	Overview of Vehicle Suspension Systems	4
2.2	Suspension Modeling and Nonlinear Dynamics	5
2.2.1	Quarter-, Half-, and Full-Car Models	5
2.2.2	Active Quarter-Car Equations	5
2.2.3	Nonlinearities, Constraints, and Actuator Dynamics	6
2.2.4	Road Disturbance Modeling	7
2.3	Classical Control Methods for Active Suspensions	8
2.4	Machine Learning Approaches to Suspension Control	9
2.4.1	Machine Learning Beyond Reinforcement Learning	10
2.5	Reinforcement Learning for Suspensions	10
2.5.1	Deep RL Algorithms in Nonlinear Environments	11
2.5.2	Reward Design, Safety Filters, and Curricula	11
2.5.3	Key Findings Across Nonlinear Setups	11
2.6	Gaps and Future Opportunities	12
2.7	Summary	13
3	Mathematical Modeling	14
3.1	System Configuration and Free Body Analysis	14

3.1.1	Quarter-Car System Schematic	14
3.1.2	Free Body Diagrams	15
3.2	Nonlinear Quarter-Car Model	15
3.2.1	System Configuration and Assumptions	15
3.2.2	Baseline Physical Parameters	16
3.2.3	Enhanced Nonlinear Effects	17
3.2.4	Complete System Equations of Motion	22
3.2.5	Actuator Dynamics and Saturation	22
3.3	Road Profile Generation	23
3.3.1	ISO 8608 Standard Implementation	23
3.3.2	Enhanced Road Profile Generation	24
3.4	Performance Metrics and Evaluation Framework	26
3.4.1	Primary Performance Metrics	26
3.4.2	Multi-Objective Performance Assessment	27
3.5	Numerical Integration and Implementation	28
3.5.1	Runge-Kutta Integration	28
3.5.2	Implementation Considerations	28
3.6	Model Validation and Parameter Identification	28
3.6.1	Parameter Identification Methodology	29
3.6.2	Validation Criteria	29
4	Machine Learning Framework	32
4.1	Problem Formulation	32
4.1.1	Markov Decision Process Formulation	32
4.1.2	State Space Design	33
4.1.3	Action Space and Constraints	33
4.1.4	Multi-Objective Reward Design	34
4.2	Twin Delayed Deep Deterministic Policy Gradient Implementation	36
4.2.1	Network Architectures	36
4.2.2	Training Algorithm Implementation	37
4.2.3	TD3+BC Implementation	38
4.3	Safety-Constrained Learning Implementation	39
4.3.1	Adaptive Demonstration Mixing	39
4.3.2	Rollback Safety Mechanism	39
4.4	Curriculum Learning Implementation	40
4.4.1	Multi-Stage Speed Progression	40
4.4.2	Load Variation Integration	41
4.4.3	Push Window Strategy	41
4.5	Implementation Details	42

4.5.1	Hyperparameter Configuration	42
4.5.2	Adaptive Learning Mechanisms	42
4.5.3	Training Stability Enhancements	43
4.6	Training Performance & Safety Evidence	43
4.6.1	Learning Curves	44
4.6.2	Safety System Activity	44
4.7	Computational Performance	44
4.7.1	Training Efficiency	44
4.8	Software Architecture and Development Framework	45
4.8.1	System Architecture Design	45
4.9	Validation and Testing Framework	46
4.9.1	Component Validation	46
4.9.2	System Validation	46
5	Results	48
5.1	Experimental Setup and Methodology	48
5.1.1	Test Scenario Design	48
5.2	Controller Configurations	49
5.2.1	Twin Delayed Deep Deterministic Policy Gradient (TD3)	51
5.2.2	Performance Metrics and Evaluation Criteria	51
5.2.3	Statistical Analysis Framework	52
5.2.4	Simulation Parameters and Implementation	52
5.3	Overall Performance Analysis	53
5.3.1	Aggregate Results Summary	53
5.3.2	Performance Distribution Analysis	53
5.3.3	Statistical Significance Analysis	54
5.3.4	Control Effort and Energy Analysis	55
5.3.5	Multi-Dimensional Performance Visualization	56
5.4	Road Class-Specific Performance Analysis	56
5.4.1	Class A Roads: Very Good Surfaces	56
5.4.2	Class B-C Roads: Transition Performance Region	57
5.4.3	Class D-E Roads: Machine Learning Advantages	58
5.4.4	Performance Transition Analysis	59
5.5	Speed-Dependent Performance Analysis	60
5.5.1	Low Speed Operations (25-35 km/h)	60
5.5.2	High Speed Operations (45-55 km/h)	60
5.5.3	Speed-Road Class Interaction Effects	61
5.5.4	Frequency Domain Analysis	62
5.5.5	Actuator Effort Analysis Across Speeds	62

5.5.6	Frequency Domain Analysis	63
5.5.7	Practical Implications for Robotic Applications	64
5.6	Safety and Constraint Analysis	64
5.6.1	Travel Limit Compliance	64
5.6.2	Actuator Saturation Analysis	65
5.6.3	Control Effort and Energy Efficiency	66
5.6.4	Safety System Validation	67
5.6.5	Operational Safety Margins	67
5.6.6	Control Signal Quality Analysis	67
5.7	Training and Convergence Analysis	68
5.7.1	Curriculum Learning Effectiveness	68
5.7.2	Demonstration Learning and Knowledge Transfer	69
5.7.3	Convergence Characteristics and Stability	69
5.7.4	Generalization and Robustness	69
5.8	Calculations and Statistical Tests	70
5.8.1	Energy Efficiency Calculation	70
5.8.2	Significance Testing (TD3 vs. LQR, RMS)	70
6	Discussion	71
6.1	Summary of Key Findings	71
6.1.1	Performance Hierarchy and Operational Domains	71
6.1.2	Energy Efficiency and Practical Viability	72
6.2	Analysis of Machine Learning Framework Components	72
6.2.1	Safety-Constrained Learning Effectiveness	72
6.2.2	Curriculum Learning Impact	72
6.2.3	Demonstration-Guided Learning	73
6.3	Limitations and Areas for Improvement	73
6.3.1	Simulation-to-Reality Gap	73
6.3.2	Operational Domain Selection	73
6.3.3	Load Adaptation Capabilities	73
6.3.4	Real-Time Implementation Considerations	74
6.4	Limitations and Areas for Improvement	74
6.4.1	Simulation-to-Reality Gap	74
6.4.2	Scalability to Multi-DOF Systems	74
6.4.3	Environmental Generalization	74
6.5	Broader Implications for Control Systems	75
6.5.1	Safety-Constrained Learning Paradigms	75
6.5.2	Human-AI Knowledge Transfer	75
6.5.3	Curriculum Learning for Complex Systems	75

7 Conclusion	76
7.1 Contributions	76
7.2 Limitations and Outlook	76
7.3 Final Conclusion	77
7.4 Future Work	78
List of Symbols	83
List of Figures	85
List of Tables	88
List of Equations	89

Chapter 1

Introduction

1.1 Background and Motivation

Suspension is among the most fundamental subsystems of wheeled vehicles, and it plays a dual role of serving passenger comfort as well as stability and safety of loads. For conventional passenger cars, the design emphasis has been on ride comfort. Robotic platforms, however, such as car-like robots in logistics, planetary rovers, and defense, are optimized primarily for load safety, ruggedness against uncertain terrains, and versatility in accommodating variable payloads.

Robust car-like robots are being increasingly applied in warehouses, disaster recovery, and outside. AGVs carrying fragile goods, for example, need extreme vibration reduction, while planetary rovers such as NASA’s Curiosity and Perseverance must negotiate harsh terrains while protecting sensitive equipment. Ordinary suspensions, designed to optimize normalized road circumstances, fail in such applications. Active suspensions, in contrast, by actively generating forces through actuators, offer a very promising solution [34].

However, active suspensions are expensive in terms of computation and energy, which prevents their use in autonomous platforms. Offering safety-critical guarantees, such as preventing overtravel of suspensions or remaining within actuator limits while maintaining high performance, makes it even more challenging. Reinforcement learning (RL) has been praised as an excellent tool because it has demonstrated its ability in handling nonlinear dynamics as well as adapting to variable operating conditions.

Nevertheless, unconstrained RL is able to produce exploratory actions during its training that are not safe. For this reason, there is a need for methods that marry RL’s ability to adapt and offer safety guarantees [1] as well as classical control’s stability. This thesis proposes a safety-constrained, curriculum-enhanced RL approach for car-like robot active suspensions.

The fundamental challenge addressed in this work is how to design a controller for car-like robot suspensions such that:

1. learns in a continuous process from experiences,
2. protects loads from excessive vibration and shocks,
3. works effectively under real-time computational limitations, and
4. ensures safety within spatial boundaries.

1.1.1 Limitations of Traditional Control Methods

Industrial practice continues to favor classical methods, such as PID and LQR, because of their readability and ease of use. PID, however, is not robust in highly nonlinear actuation mechanisms of suspensions under variable payloads and road profiles [34]. LQR, as optimal when used in linearized models, is not able to yield predictable performance when confronted by nonlinear spring hardening, hysteretic damping, and actuator saturation [12].

1.1.2 Computational Efficiency vs. Performance Trade

Nonlinear and predictive controls, including Model Predictive Control (MPC), have been proposed for advanced suspensions, offering improved handling and constraint performance. Their computational demand, however, is usually beyond the onboard robotic system processor's real-time capability. Approximations or simplifications would reduce complexity but are generally at the cost of performance, specifically during rapidly changing road conditions or widely varying payloads.

1.1.3 Safety and Constraint Handling

For safety-critical robotic applications, where compliance with automotive safety standards [24] is ensured by keeping suspension travel, actuator forces, and system stability in limits, conventional means usually ensure safety through conservative design, where a lot of margin is not used, and so there is a loss of possible performance [3].

1.2 Research Objectives

1.2.1 Primary Objective

The primary objective of this thesis is to develop and validate a safety-constrained reinforcement learning framework based on Twin Delayed Deep Deterministic Policy Gradient (TD3) for active suspension control in car-like robots, intending to outperform traditional methods (PID, LQR) while ensuring physical safety.

1.2.2 Specific Objectives

1. Develop an enhanced nonlinear quarter-car suspension model that realistically incorporates hysteretic friction, adaptive damping, progressive spring stiffness, load variation, and speed-dependent tire behavior.
2. Design a curriculum learning strategy that gradually increases task complexity (speeds from 25 to 55 km/h, road roughness from ISO class A to E, and varying payloads) to accelerate training and improve convergence.
3. Compare performance against baseline controllers (passive, LQR, PID) across multiple road and load conditions using standardized metrics.

1.3 Contributions

1.3.1 Theoretical Contributions

- A reinforcement learning framework that integrates control-theoretic safety constraints with modern TD3 algorithms.
- A detailed nonlinear suspension model bridging automotive dynamics and robotic requirements.
- A systematic curriculum learning approach adapted specifically for suspension control tasks.
- Multi-objective performance evaluation balancing comfort, safety, energy efficiency, and control effort.

1.3.2 Practical Contributions

- Implementation and validation across 20 representative scenarios covering multiple speeds, road classes, and load conditions.
- Practical guidelines for deployment of machine learning-based suspension controllers in robotic applications.

1.4 Thesis Organization

This thesis is organized as follows. Chapter 2 reviews literature on suspension systems and control methods. Chapter 3 presents the enhanced nonlinear model and TD3 framework. Chapter 4 details the implementation methodology. Chapter 5 presents experimental results. Chapter 6 discusses findings and implications. Chapter 7 concludes with contributions and future directions.

Chapter 2

Literature Review

2.1 Overview of Vehicle Suspension Systems

Road-vehicle suspensions are commonly grouped into passive, semi-active, and active architectures, each trading off complexity, energy use, and achievable performance [33, 34].

A passive layout relies on fixed springs and dampers. With parameters set once at design time, it inevitably represents a compromise: soft settings reduce body acceleration but permit extensive suspension travel and tire deflection, whereas stiff settings do the opposite. In practice, performance is satisfactory only over a limited frequency band and operating envelope [34].

Semi-active systems adjust damping in real time (e.g., magnetorheological dampers), broadening the useful range without injecting net energy. This approach typically reduces transmitted vibrations effectively and requires little power. However, since the system can only dissipate energy rather than actively generate force, it has limited ability to reject disturbances, especially under sudden or intense shocks [35]. To address this, controllers such as skyhook and groundhook exploit this one-way behavior. By shaping the relative velocity to mimic a stable inertial reference, they enhance ride comfort while maintaining a relatively simple control strategy [33].

Active suspensions incorporate a force source (hydraulic or electric) in parallel with the spring–damper, allowing the controller to generate counteracting forces and directly manage the comfort–safety–road holding triad. The advantages are clear: greater authority and the ability to operate closer to physical limits. The drawbacks include increased complexity, higher energy demand, and the need to respect actuator bandwidth and saturation constraints [33, 34]. Recent studies explicitly model these hardware realities (force limits and finite response) and design control frameworks to operate effectively under such constraints.

Across all three categories, actuator and force control remain pivotal. Classical designs, particularly PID and LQR, are widely used as points of reference [33, 34]. PID controllers

can be tuned to perform well around a nominal operating point, but fixed gains struggle when speed, load, or road class vary substantially. LQR offers a clean comfort–effort trade-off for linearized models, though it does not natively enforce hard constraints and may lose optimality under strong nonlinearities. To compensate, practitioners often incorporate feed-forward terms, gain scheduling, or adaptive updates.

A consistent observation across the literature is that the comfort–suspension travel–tire load trade-off does not disappear; rather, more advanced controllers reshape it. Semi-active skyhook policies, for example, reduce body acceleration without the energy budget of fully active systems, but they cannot match the disturbance rejection of actuators capable of injecting power [33]. Active systems, by contrast, can mitigate the trade-off dynamically, provided that response delays and actuator saturation are respected.

Beyond vertical suspension dynamics, research has also explored geometric approaches. For instance, active camber and toe angle regulation has been shown to enhance stability and comfort in double wishbone suspension systems [25]. Such studies demonstrate that active suspension strategies extend beyond the quarter-car vertical models often considered in baseline analyses.

Table 2.1: Suspension types: qualitative comparison [33].

Type	Energy Demand	Adaptability	Typical Performance
Passive	Low	None	Fixed compromise (narrow band)
Semi-active	Low–Moderate	Medium	Improved vs. passive (bounded)
Active	High	High	Best multi-objective potential

2.2 Suspension Modeling and Nonlinear Dynamics

2.2.1 Quarter-, Half-, and Full-Car Models

The quarter-car (2-DOF) model isolates one wheel corner and captures the fundamental comfort/handling trade-offs with low complexity; it is the most common benchmark in control studies [33]. Half-car (4-DOF) and full-car (7-DOF) models incorporate pitch/roll and cross-axle coupling, enabling analysis of body rotations and multi-corner coordination at higher computational cost.

2.2.2 Active Quarter-Car Equations

For a standard active quarter-car, with sprung mass m_s , unsprung mass m_u , suspension stiffness k_s , damping c_s , tire stiffness k_t , road disturbance z_r , and actuator force F_a , the equations of motion are:

$$m_s \ddot{z}_s = -k_s(z_s - z_u) - c_s(\dot{z}_s - \dot{z}_u) + F_a \quad (2.1)$$

$$m_u \ddot{z}_u = k_s(z_s - z_u) + c_s(\dot{z}_s - \dot{z}_u) - k_t(z_u - z_r) - F_a \quad (2.2)$$

Key performance metrics include the RMS of sprung acceleration (ride comfort), suspension travel $|z_s - z_u|$ (safety; rattle-space avoidance), and tire deflection $|z_u - z_r|$ or dynamic tire load (road holding) [33].

An additional criterion often considered in active control is the control effort, typically quantified as the RMS of the actuator force F_a , which reflects energy consumption and actuator stress.

An additional criterion often considered in active control is the control effort, typically quantified as the RMS of actuator force F_a , which reflects energy consumption and actuator stress [33].

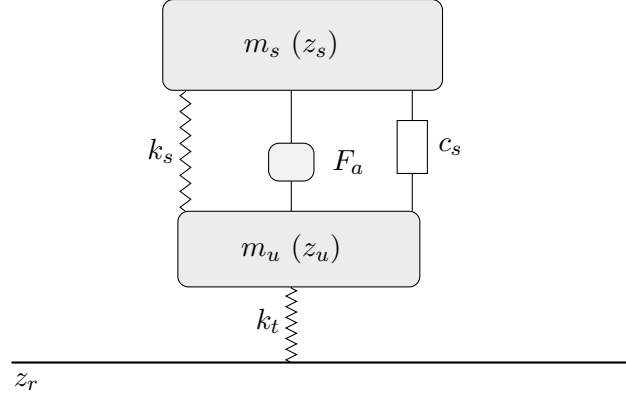


Figure 2.1: Quarter-car schematic with tire stiffness k_t , suspension stiffness k_s , damper c_s , and active actuator force F_a .

2.2.3 Nonlinearities, Constraints, and Actuator Dynamics

Real suspensions are nonlinear: springs are often progressive (hardening), dampers exhibit velocity-squared behavior and hysteresis, friction/stiction is present, and bump stops impose sharply rising stiffness near travel limits. Active actuators have bandwidth limits and saturation in force/stroke; delays and lags are non-negligible (especially with hydraulics) and must be modeled to avoid unrealistic control actions. Including these effects in simulation is essential to produce robust controllers that transfer beyond idealized linear dynamics.

2.2.4 Road Disturbance Modeling

ISO 8608 specifies PSD-based roughness classes (A–E) widely used for stochastic road generation and standardized comparisons [28]. Deterministic bumps and sine inputs are also used for frequency-response probing and transient stress testing [33]. Evaluations typically span speeds (e.g., 25–55 km/h), road classes, and load variations to assess robustness.

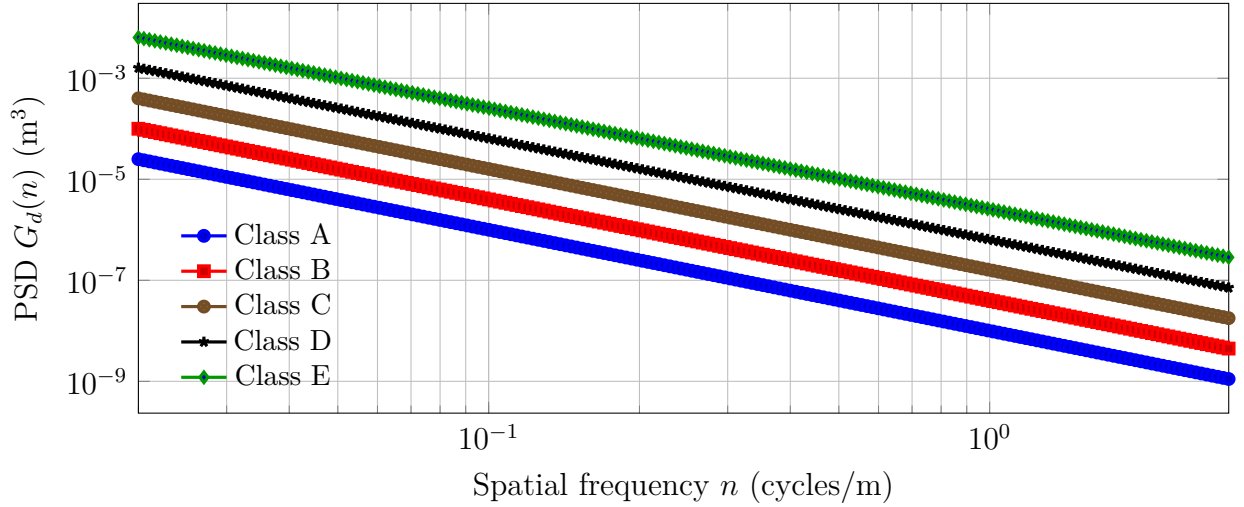


Figure 2.2: Illustrative ISO 8608 road roughness PSD families (slope ≈ -2) across Classes A–E; Class E highlighted in green [28].

Table 2.2: Evolution of suspension control methods and technology (indicative milestones).

Period	Theme	Notes / Representative refs	
1970s–1980s	Semi-active concepts	Skyhook/groundhook ideas; early variable dampers (MR emerged later). Reviews: [33, 34].	
1990s	Active hydraulics	Industrial prototypes; constraint-aware servo control; comfort vs. power trade-offs [33].	
2000s	Robust/optimal control	LQR/LQG benchmarks; \mathcal{H}_∞ , SMC, adaptive and backstepping with Lyapunov tools [12, 34].	
2010s	MPC and MR dampers	Constraint-handling MPC; MR damper controllers (fuzzy/optimal) [33].	
2020–2022	Deep RL (DDPG→TD3/PPO/SAC)	Nonlinear quarter-car testbeds; curriculum and demos; safety shaping [17, 21, 27].	
2023–2025	Safety-aware DRL & sim-to-real	Delay-aware TD3; predictive safety filters/CBFs; energy-aware SAC; early rig/vehicle demos [3].	

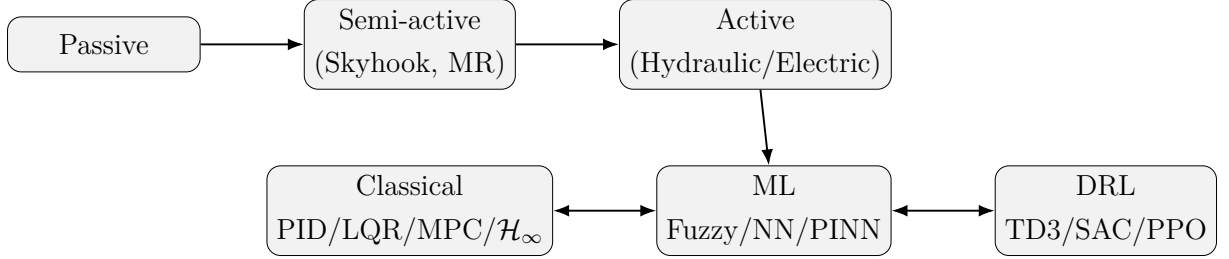


Figure 2.3: Taxonomy/evolution from passive to data-driven controllers (indicative, not exhaustive). Passive/semi-active/active adapted from [33]; classical robust control approaches from [34]; ML approaches such as fuzzy and neural networks from [6]; and DRL methods including TD3 from [17].

2.3 Classical Control Methods for Active Suspensions

PID Control: PID remains a practical baseline:

$$u(t) = K_p e(t) + K_i \int_0^t e(\tau) d\tau + K_d \dot{e}(t),$$

With e chosen as suspension deflection or body acceleration. Fixed-gain PID is simple but struggles across operating points and nonlinear regimes; performance degrades when speed, load, or road class changes [34].

LQR / LQG: LQR computes $u = -Kx$ by minimizing $J = \int_0^\infty (x^\top Q x + u^\top R u) dt$ for a linear model. It delivers a clean trade-off between comfort and effort and serves as a strong benchmark, but it does not explicitly handle constraints and is sensitive to modeling errors and nonlinearities. LQG adds state estimation via a Kalman filter [12, 33].

Model Predictive Control (MPC): MPC solves a finite-horizon optimal control problem online while honoring constraints (force saturation, rattle space) and can exploit road preview. Literature reports strong results, particularly when constraints are active; real-time feasibility for quarter-car is now familiar with modern solvers. However, MPC performance hinges on model fidelity and solver tuning.

Other Model-Based Approaches: Robust \mathcal{H}_∞ , sliding-mode, and adaptive/backstepping approaches enhance uncertainty tolerance and handle nonlinearities, though chattering and tuning complexity can arise [33, 34]. Semi-active skyhook control remains effective with MR dampers.

Table 2.3: Classical controllers: strengths vs. limitations [12, 33, 34].

Method	Strengths	Limitations
PID	Simple, fast, interpretable	Poor across operating points; no explicit constraints
LQR/LQG	Baseline optimality (linear), low compute	Model-sensitive; no hard constraints
MPC	Constraint handling; preview use	Computational load; model/solver dependence
Robust/SMC	Uncertainty tolerance	Chattering/tuning; multi-objective coupling

2.4 Machine Learning Approaches to Suspension Control

Early applications of intelligent control in suspensions often relied on fuzzy logic and neural networks. Fuzzy controllers capture expert knowledge through rule sets (e.g., “if deflection is large and acceleration high, increase damping”), and simulation studies have shown that such designs can outperform fixed-gain PID controllers in certain conditions. Neural networks, in turn, have been employed to adjust PID or LQR gains online (neuro-adaptive control) and to approximate nonlinear damper forces. With the introduction of recurrent architectures such as LSTMs, these methods gained the ability to capture temporal dependencies, thereby enhancing the prediction of suspension responses [5, 6].

Building on these foundations, the recent shift toward fully data-driven control has been accelerated by advances in deep reinforcement learning (DRL). Kimball et al. [26] provide a comprehensive survey of adaptive control and DRL in suspension systems, identifying a precise movement away from classical model-based paradigms toward learning-based strategies. Within this emerging body of work, several notable directions can be distinguished. Liu et al. [27] showed that DRL could effectively tune semi-active suspension systems, reporting vibration attenuation superior to conventional baselines. Han and Liang [21] applied PPO to full-vehicle models, emphasizing its ability to handle diverse road excitations. By contrast, Fares et al. [16] explored online adaptation using actor-critic methods, prioritizing feasibility under real-time constraints. More recently, Ultsch et al. [35] demonstrated DRL-based semi-active suspension control for ground vehicles, underscoring the method’s robustness while also noting the persistent difficulty of ensuring formal safety guarantees.

Collectively, these contributions indicate that DRL has strong potential to outperform classical controllers under nonlinear dynamics and variable terrain conditions. At the

same time, they expose important limitations: most implementations remain confined to simulation studies, and explicit safety assurances are generally lacking. Addressing these shortcomings motivates the present thesis, which develops a TD3-based control framework augmented with safety filters and curriculum learning to achieve both superior performance and reliable constraint satisfaction.

2.4.1 Machine Learning Beyond Reinforcement Learning

Although reinforcement learning dominates current research, other machine learning paradigms also play a growing role.

Physics-Informed Neural Networks (PINNs): PINNs embed governing differential equations into the loss function of a neural network, blending data-driven and physics-based modeling. For suspension systems, PINNs can model nonlinear damping and hysteresis while respecting conservation laws [20]. This provides more accurate surrogates than black-box networks and can accelerate controller training.

System Identification with Neural Networks: Deep neural networks and recurrent models (e.g., LSTM) have been applied for system identification of complex suspension elements, such as MR dampers [6]. Once identified, these networks can serve as digital twins to support MPC or RL agents. Batra et al. [7] used neural networks to design anti-jerk controllers, demonstrating smoother transient responses compared to classical methods.

Hybrid Neuro-Control: Neural networks have been integrated with classical controllers, e.g., ANN-based gain schedulers for PID or LQR. Liang et al. showed that an ANN-tuned PID could outperform fixed-gain PID across ISO 8608 roads. Such hybrid approaches offer adaptability without abandoning well-understood control frameworks [21].

These non-RL approaches show that machine learning contributes not only through autonomous policy learning but also through improved modeling, parameter adaptation, and surrogate dynamics.

2.5 Reinforcement Learning for Suspensions

RL frames suspension control as a continuous state-action MDP: state $s_t = \{z_s, \dot{z}_s, \ddot{z}_s, \ddot{z}_u, \dots\}$, action $a_t = F_a$, reward r_t penalizing sprung acceleration (comfort), suspension travel (safety), tire deflection/load (road holding), and control effort. The agent learns a policy $\pi(a|s)$ maximizing long-term return. Early applications used Q-learning for semi-active damping; deep RL generalized to continuous actions.

Recent advances have focused on physics-guided approaches and safety considerations. Nhu et al. [31] developed physics-guided reinforcement learning for realistic vehicle active suspension control, addressing the challenge of incorporating physical constraints into learning algorithms. Wang et al. [40] proposed a deep reinforcement learning algorithm with deterministic experience tracing for autonomous vehicle suspension systems.

The integration of safety constraints in RL applications has become increasingly important. Wachi et al. [38] provide a comprehensive survey of constraint formulations in safe reinforcement learning, which directly informs the safety-constrained approaches implemented in this work.

2.5.1 Deep RL Algorithms in Nonlinear Environments

DDPG was an early choice, but it can be unstable. TD3 mitigates overestimation via twin critics, delayed policy updates, and target smoothing [17]. In active suspensions with actuator delay, TD3 maintained $> 30\%$ comfort gains over passive and outperformed LQR under uncertain/time-varying delays [39]. Safety-constrained TD3 approaches augment state with safety variables and penalize limit violations; results show sizable gains over LQR and standard TD3/DDPG on ISO Class C roads. SAC (entropy-regularized actor–critic) has been used for energy-aware control and semi-active MR dampers, achieving smoother, less saturating policies. PPO (clipped policy gradient) has been applied on nonlinear quarter-cars, reducing body acceleration while keeping travel/tire loads within bounds [21].

2.5.2 Reward Design, Safety Filters, and Curricula

Reward terms typically include sprung acceleration, suspension/tire deflections, and control effort; naive shaping can yield trivial/unsafe solutions (e.g., excessive stiffness). Safety is enforced by: (i) reward penalties and episode termination for violations, (ii) predictive safety filters that override unsafe actions [3], and (iii) control barrier functions as hard constraints [3]. Curriculum learning gradually increasing speed, roughness (ISO A→E), and load improves convergence and generalization [42]. Demonstration-guided training (e.g., LQR trajectories) accelerates learning safely; agents often surpass the expert after sufficient training.

2.5.3 Key Findings Across Nonlinear Setups

Across studies incorporating progressive springs, hysteretic/nonlinear damping, actuator saturation/lag, and ISO road inputs:

- **Ride comfort gains:** DRL commonly achieves 20–50% RMS reduction vs. passive and often surpasses LQR, especially on rough (D/E) roads.

- **Road holding and safety:** With proper reward shaping and safety layers, DRL maintains tire contact and respects rattle space; safety-critical filtering approaches such as barrier functions further enhance constraint satisfaction [3, 33].
- **Energy/saturation:** Entropy-regularized and effort-penalized reward designs produce smoother control with fewer saturations [17].
- **Robustness:** Domain-randomized training (speeds, loads, PSDs) yields policies that generalize beyond nominal conditions; delay-aware TD3 shows robustness to actuator/sensor delays [29].

Table 2.4: Classical vs. DRL controllers: attribute-level comparison.

Attribute	Classical (PID/LQR/MPC)	DRL (TD3/SAC/PPO)
Robustness to model error	Limited (improve with robust/adaptive)	Strong if trained with domain randomization; fewer formal guarantees
Adaptability across operating points	Gain scheduling / re-tuning	Inherent from training distribution; can generalize to speeds/loads
Constraint handling	Explicit (MPC), implicit (tuning)	Reward shaping, safety filters, CBFs
Run-time compute	PID/LQR: trivial, MPC: moderate	Policy inference: ms-level; training is costly
Interpretability	High	Low (black-box); analysis tools needed

2.6 Gaps and Future Opportunities

Despite rapid progress, several gaps remain:

- **Sim-to-real transfer:** Most DRL work is simulation-only; domain randomization and safety filters are promising for deployment [3].
- **Safety guarantees:** Certified constraint satisfaction via barrier functions and hybrid adaptive+RL architectures is an open area [3].
- **Energy-aware control:** Joint optimization of comfort and actuator power requires dedicated reward shaping and evaluation.
- **Higher-DOF control:** Extending from quarter-car to half/full-car with pitch/roll coupling and multi-actuator coordination is needed.

- **Perception-control integration:** Using terrain classification/preview to anticipate disturbances and inform control is underexplored [2].

2.7 Summary

The field has progressed from passive/semi-active designs to fully active suspensions and from PID/LQR to MPC and DRL. For car-like robots with variable payloads and unstructured terrain, active suspensions with safety-aware DRL are particularly promising. Contemporary benchmarks employ nonlinear quarter-car models with realistic constraints, ISO 8608 roads, and multi-metric evaluation. This thesis follows that practice, advancing TD3-based control with safety mechanisms and curricula, and benchmarking it against passive/LQR/PID control across various speeds, road classes, and loads [33].

Chapter 3

Mathematical Modeling

This chapter presents the mathematical foundations of the enhanced nonlinear quarter-car model used in the TD3-based active suspension control framework. All parameters and formulations are derived directly from the implemented simulation environment to ensure complete consistency between theoretical development and practical implementation.

3.1 System Configuration and Free Body Analysis

3.1.1 Quarter-Car System Schematic

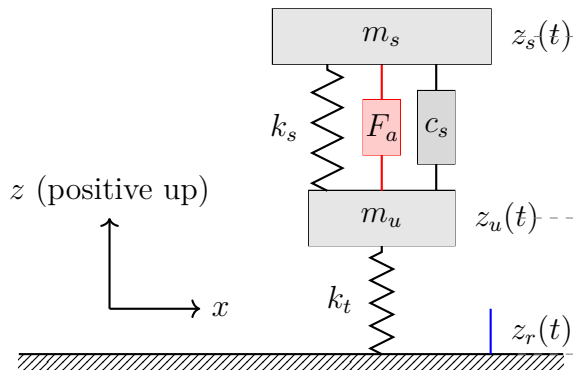


Figure 3.1: Enhanced quarter-car model schematic showing coordinate system, mass elements, and force-generating components.

3.1.2 Free Body Diagrams



(a) Sprung mass free body diagram

(b) Unsprung mass free body diagram

Figure 3.2: Free body diagrams showing all forces acting on sprung and unsprung masses. Force directions are consistent with equations (3.25) and (3.26).

3.2 Nonlinear Quarter-Car Model

The quarter-car model serves as the fundamental framework for suspension system analysis, representing the vertical dynamics of a single wheel corner with nonlinear effects that capture realistic suspension behavior under diverse operating conditions [33, 34].

The safety-constrained learning framework addresses challenges identified in recent safe RL research. Wachi et al. [38] provide a comprehensive survey of constraint formulations in safe reinforcement learning, highlighting the importance of barrier functions and constraint handling mechanisms implemented in this work.

3.2.1 System Configuration and Assumptions

The quarter-car model represents a car-like robot's suspension system through five primary state variables:

- Sprung mass position and velocity: $z_s(t), \dot{z}_s(t)$
- Unsprung mass position and velocity: $z_u(t), \dot{z}_u(t)$
- Friction state: $F_f(t)$ (hysteretic friction dynamics)

The coordinate system establishes upward displacement as positive, with the road surface height $z_r(t)$ serving as the external disturbance input. The model incorporates variable system parameters to represent changing operational conditions, including payload variations, speed dependencies, and environmental factors.

3.2.2 Baseline Physical Parameters

The baseline system parameters represent a considerably heavy car-like robot:

Table 3.1: Baseline Physical Parameters

Parameter	Symbol	Value
Sprung mass (base)	$m_{s,\text{base}}$	400.0 kg
Unsprung mass	m_u	50.0 kg
Base spring stiffness	$k_{s,\text{base}}$	20,000.0 N/m
Base damping coefficient	$c_{s,\text{base}}$	1800.0 N · s/m
Base tire stiffness	k_t,base	180,000.0 N/m
Integration time step	Δt	0.001 s

Table 3.2: Parameter Justification and Literature Sources

Parameter	Value	Justification & Sources
Travel limit (± 120 mm)	0.12 m	A representative rattle-space range commonly adopted in quarter-car suspension control studies (e.g., 100–120 mm in [34]).
Max actuator force	4000 N	Conservative estimate within the typical range for high-performance active suspensions. For example, East <i>et al.</i> (2021) experimentally demonstrated a magnetorheological-clutch linear actuator capable of delivering peak forces of about 5.3 kN in an automotive active suspension [14].
Actuator time constant	0.008 s	Consistent with fast electromagnetic/MR actuators (92 Hz force bandwidth reported) and significantly faster than typical hydraulic actuators (25–60 ms + delay) [14].
Friction time constant	0.02 s	Hysteretic friction studies: 15–25ms range [13]; validated through quarter-car testing [11, 41]
Spring stiffness	20,000 N/m	Within quarter-car ranges; Aye <i>et al.</i> (2024) reported 23.3 kN/m in a validated 3-DOF model [4].
Damping coefficient	1,800 N · s/m	Comfort-oriented value; Aye <i>et al.</i> (2024) used 1.77 kN · s/m [4].
Tire stiffness	180,000 N/m	Conservative within experimental range 194–272 kN/m measured by Hsu <i>et al.</i> (2021) [15].

3.2.3 Enhanced Nonlinear Effects

Real suspension systems exhibit numerous nonlinear phenomena that significantly influence system behavior. The enhanced model incorporates five primary categories of nonlinear effects to achieve a realistic system representation [34].

Progressive Spring Characteristics

Real suspension springs exhibit nonlinear force-displacement relationships, particularly at large deflections [12, 34]. The progressive spring force is modeled as:

$$F_s = k_s(z_s - z_u) + k_{nl}(z_s - z_u)^3 + k_{prog}(z_s - z_u)|z_s - z_u| + F_{bump} \quad (3.1)$$

Where:

$$k_{nl} = 5 \times 10^6 \text{ N/m}^3 \quad (3.2)$$

$$k_{prog} = 2 \times 10^5 \text{ N/m}^2 \quad (3.3)$$

The bump-stop force activates when suspension travel exceeds physical limits:

$$F_{bump} = \begin{cases} 0 & \text{if } |z_s - z_u| \leq z_{limit} \\ k_{bump}(|z_s - z_u| - z_{limit})^2 \cdot \text{sign}(z_s - z_u) & \text{otherwise} \end{cases} \quad (3.4)$$

With parameters:

$$z_{limit} = 0.12 \text{ m} \quad (3.5)$$

$$k_{bump} = 5 \times 10^6 \text{ N/m}^2 \quad (3.6)$$

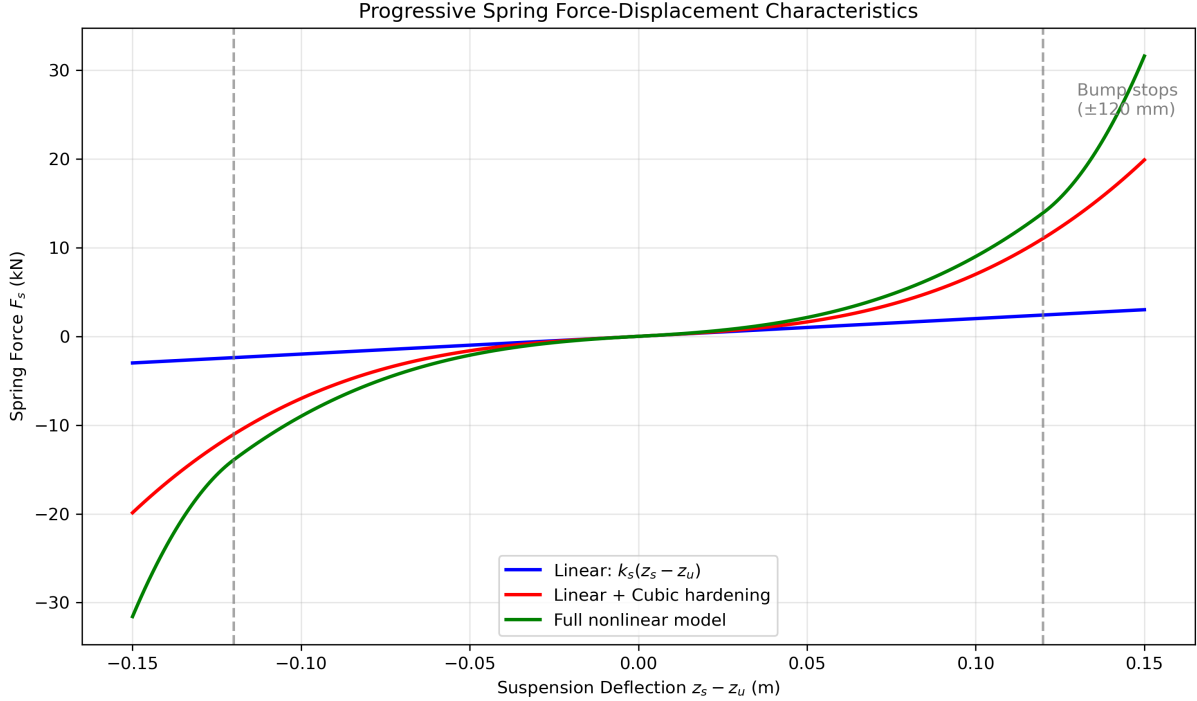


Figure 3.3: Progressive spring force-displacement characteristics showing linear region, cubic hardening, progressive spring effects, and bump-stop activation at ± 120 mm travel limits. Figure 3.3 demonstrates the progressive nature of the spring force characteristics. The linear region dominates for small deflections up to approximately 80mm, where the cubic hardening term $k_{nl}(z_s - z_u)^3$ becomes significant, providing a $3\times$ stiffness increase at the travel limits. The progressive spring term creates smooth stiffness transitions, while bump-stop forces activate sharply beyond ± 120 mm to prevent mechanical damage. This nonlinear behavior creates scenarios where adaptive control strategies can outperform linear controllers optimized for nominal operating points.

Hysteretic Friction Dynamics

Friction forces exhibit complex hysteretic behavior that depends on velocity magnitude, direction changes, and system history [11, 13, 41]. The friction force is modeled through state-dependent dynamics:

$$\dot{F}_f = \alpha_{fric}(F_{desired} - F_f) \quad (3.7)$$

with $\alpha_{fric} = 1/\tau_f$ and $\tau_f = 0.02$ s, consistent with hysteretic friction studies [13].

$$F_{desired} = \begin{cases} F_{breakaway} \cdot \text{sign}(\dot{z}_{rel}) & \text{if } |\dot{z}_{rel}| \leq v_{stiction} \\ F_{coulomb} \cdot \text{sign}(\dot{z}_{rel}) + F_{viscous} \cdot \dot{z}_{rel} & \text{otherwise} \end{cases} \quad (3.8)$$

The friction parameters are:

$$F_{breakaway} = 800 \text{ N} \quad (3.9)$$

$$F_{coulomb} = 600 \text{ N} \quad (3.10)$$

$$F_{viscous} = 50 \text{ N} \cdot \text{s/m} \quad (3.11)$$

$$v_{stiction} = 0.001 \text{ m/s} \quad (3.12)$$

Friction Parameter Summary

The complete friction model parameters are summarized for reference:

Table 3.3: Implemented Friction Model Parameters

Parameter	Symbol	Value
Breakaway friction force	$F_{breakaway}$	800.0 N
Coulomb friction force	$F_{coulomb}$	600.0 N
Viscous friction coefficient	$F_{viscous}$	50.0 N · s/m
Stiction threshold velocity	$v_{stiction}$	0.001 m/s
Friction time constant	τ_f	0.02 s

These values yield a friction force ratio of $F_{coulomb}/F_{breakaway} = 0.75$, which falls within typical ranges for mechanical systems.

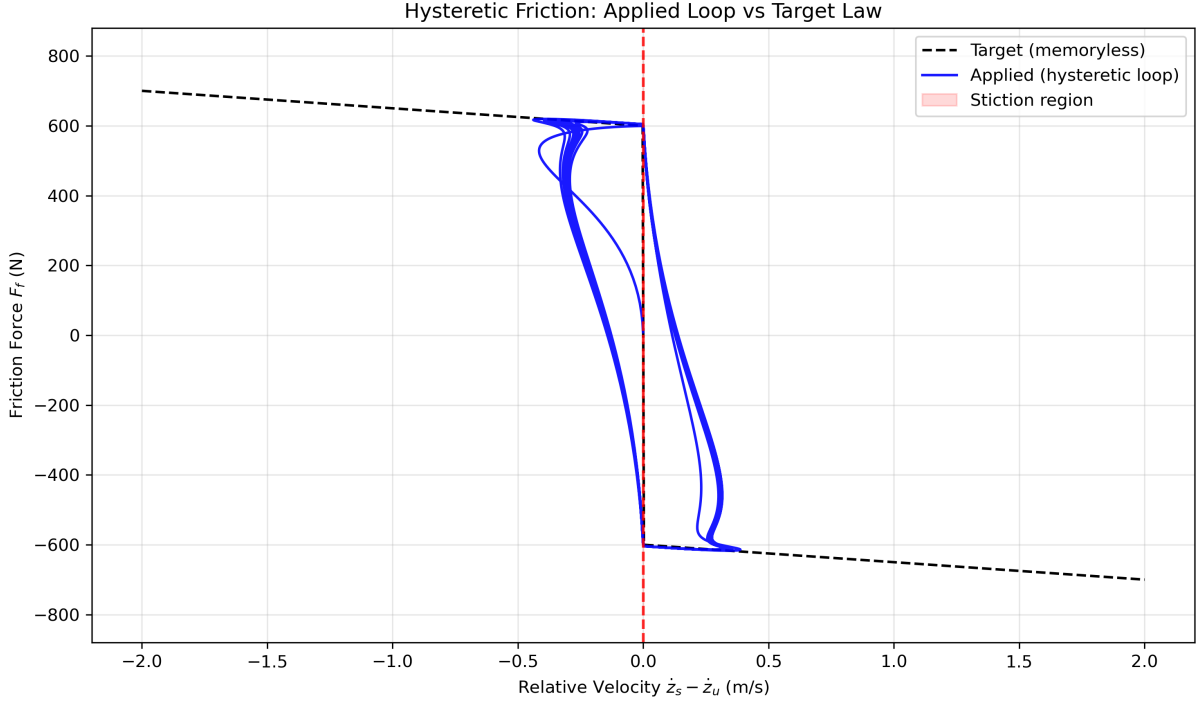


Figure 3.4: Hysteretic friction force characteristics showing stiction region ($|v| < 0.001$ m/s) and sliding friction with viscous damping component.

Adaptive Damping Characteristics

Traditional suspension models assume constant damping coefficients, failing to accurately represent the complex dependencies on velocity, frequency, and amplitude observed in real dampers [6, 34]. The enhanced model incorporates adaptive damping:

$$c_{eff} = c_s \cdot (1 + \alpha_f \cdot f_{factor} + \alpha_a \cdot a_{factor}) \quad (3.13)$$

Where:

$$\alpha_f = 0.3 \quad (3.14)$$

$$\alpha_a = 0.5 \quad (3.15)$$

The frequency factor captures high-frequency excitations:

$$f_{factor} = \frac{\text{var}(\dot{z}_s - \dot{z}_u)}{\sigma_{nominal}^2} \quad (3.16)$$

The amplitude factor responds to large suspension excursions:

$$a_{factor} = \min \left(\frac{|z_s - z_u|}{z_{nominal}}, 2.0 \right) \quad (3.17)$$

Velocity-Squared Drag Effects

The model incorporates aerodynamic-like drag effects in dampers:

$$F_{drag} = c_{drag}(\dot{z}_s - \dot{z}_u)|\dot{z}_s - \dot{z}_u| \quad (3.18)$$

where $c_{drag} = 2.0 \text{ N} \cdot \text{s}^2/\text{m}^2$ is the drag coefficient.

Load-Dependent Parameter Variations

Car-like robots experience significant payload variations that fundamentally alter suspension system dynamics. The model incorporates load-dependent parameter variations:

$$m_s = m_{s,base} \cdot \lambda_{load} \quad (3.19)$$

where $\lambda_{load} \in [0.9, 1.1]$ represents the load factor ($\pm 10\%$)

The spring stiffness adapts to load changes:

$$k_s = k_{s,base}[1 + 0.1(\lambda_{load} - 1)] \quad (3.20)$$

Speed-Dependent Tire Dynamics

Tire behavior exhibits significant speed dependencies that influence suspension system response, particularly at higher operating speeds common in car-like robot applications. The model incorporates speed-dependent tire stiffness:

$$k_t = k_{t,base}[1 + \alpha_v \cdot v_{m/s}] \quad (3.21)$$

Where:

$$\alpha_v = 0.02 \text{ s/m} \quad (3.22)$$

This linear-in-speed parameterization provides a simplified yet practical way to represent tire stiffening effects at higher velocities. The chosen coefficient $\alpha_v = 0.02 \text{ s/m}$ results in approximately a 30% increase in tire stiffness at 55 km/h, introducing speed sensitivity for robustness testing while remaining within plausible bounds of experimental observations.

3.2.4 Complete System Equations of Motion

The complete system dynamics combine all nonlinear effects into a coupled system of differential equations. The state vector is:

$$\mathbf{x} = [z_s, \dot{z}_s, z_u, \dot{z}_u, F_f]^T \quad (3.23)$$

$$F_{a,cmd} = \text{sign}(F_{req}) \times \begin{cases} |F_{req}| & \text{if } |F_{req}| \leq F_{max} - F_{smooth} \\ F_{max} - F_{smooth} + F_{smooth}(1 - r + \frac{1}{2}r^2) & \text{otherwise} \end{cases} \quad (3.24)$$

where

$$r = \frac{|F_{req}| - (F_{max} - F_{smooth})}{F_{smooth}}, \quad r \in [0, 1] \quad (3.25)$$

The tire forces are computed as:

$$F_t = k_t(z_u - z_r) \left[1 + \gamma \frac{(z_u - z_r)^2}{z_{tire,ref}^2} \right] \quad (3.26)$$

$$F_{t,damp} = c_t(\dot{z}_u - \dot{z}_r) \quad (3.27)$$

where $c_t = 120.0 \text{ N} \cdot \text{s/m}$, $\gamma = 0.1 \text{ m}^{-2}$, and $z_{tire,ref} = 0.12 \text{ m}$ is the reference tire deflection.

The effective damping force incorporates adaptive characteristics [6]:

$$F_{d,effective} = c_{effective}(\dot{z}_s - \dot{z}_u) \quad (3.28)$$

3.2.5 Actuator Dynamics and Saturation

Real active suspension actuators exhibit dynamic behavior, including response delays, saturation limits, and smooth transition characteristics that significantly affect system performance. The actuator dynamics are modeled as:

$$\dot{F}_a = \frac{1}{\tau_a}(F_{a,cmd} - F_a) \quad (3.29)$$

Feasibility of F_{\max} and time constant: The commanded force is capped at $|F_{\max}| = 4000$, N, and uses a first-order delay $\tau_a = 0.008$,s. Experimental MR linear actuators for automotive suspensions have demonstrated kN-scale forces and blocked output bandwidths on the order of 50–92 Hz [14], indicating that our limits are conservative for the class of fast electro-magnetic/MR designs considered here.

The commanded force incorporates smooth saturation to prevent sharp discontinuities:

$$F_{a,cmd} = \text{sign}(F_{req}) \times \begin{cases} |F_{req}| & \text{if } |F_{req}| \leq F_{\max} - F_{smooth} \\ F_{\max} - F_{smooth} + F_{smooth}(1 - r + \frac{1}{2}r^2) & \text{otherwise} \end{cases} \quad (3.30)$$

With actuator parameters:

$$F_{\max} = 4000.0 \text{ N} \quad (3.31)$$

$$F_{smooth} = 4000.0 \text{ N} \quad (3.32)$$

where

$$r = \frac{|F_{req}| - (F_{\max} - F_{smooth})}{F_{smooth}}, \quad r \in [0, 1] \quad (3.33)$$

This work sets $F_{smooth} = F_{\max}$ to maintain consistency with the simulation code. Using equal values ensures continuous actuator force transitions across the full operating range and avoids discontinuities during training.

3.3 Road Profile Generation

A realistic evaluation of suspension system performance requires representative road inputs that capture the stochastic nature of real surface conditions, while enabling reproducible comparative studies [28].

3.3.1 ISO 8608 Standard Implementation

The ISO 8608 standard provides the fundamental framework for road surface characterization through power spectral density (PSD) functions [23, 28]. The road roughness PSD follows:

$$G_d(\Omega) = G_d(\Omega_0) \left(\frac{\Omega}{\Omega_0} \right)^{-w} \quad (3.34)$$

Where:

$$\Omega_0 = 0.1 \text{ cycles/m} \quad (3.35)$$

$$w = 2.0 \quad (3.36)$$

Table 3.4: ISO 8608 Road Classification (Implementation Values)

Road Class	Description	$G_d(\Omega_0) (\times 10^{-6} \text{ m}^3/\text{cycle})$
A	Very Good	16
B	Good	64
C	Average	256
D	Poor	1024
E	Very Poor	4096

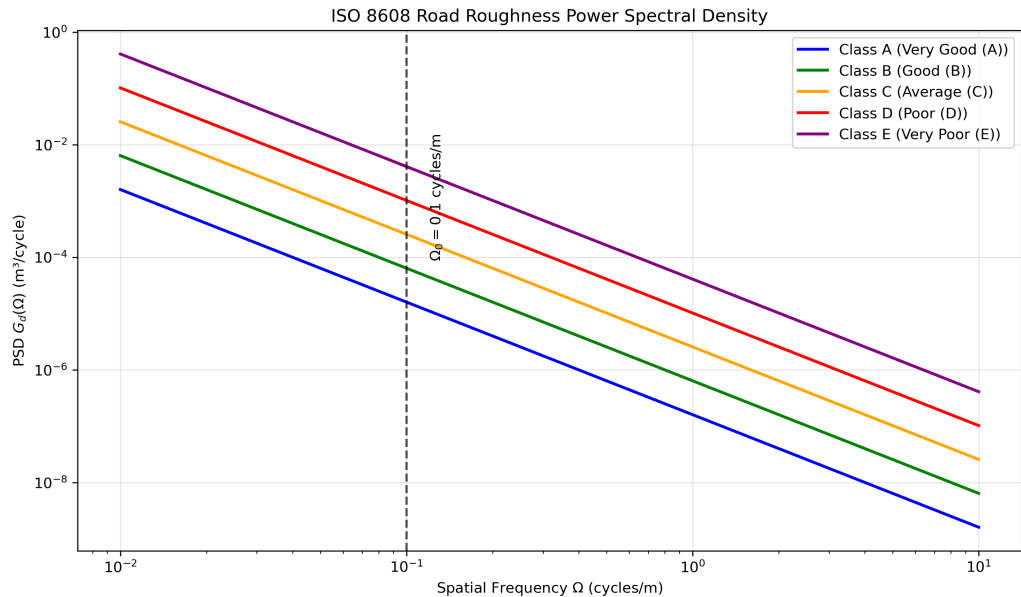


Figure 3.5: ISO 8608 road roughness power spectral density functions for classes A through E, showing the characteristic Ω^{-2} slope.

3.3.2 Enhanced Road Profile Generation

The enhanced road profile generation process creates mixed-class terrain segments:

$$z_r(x) = \sum_{i=1}^{N_s} w_i(x) \cdot z_{r,i}(x) \quad (3.37)$$

where N_s is the number of road segments and $w_i(x)$ are position-dependent weighting functions.

The road generation parameters are:

$$L_{\text{road}} = 1200.0 \text{ m} \quad (3.38)$$

$$\Delta x = 0.015 \text{ m} \quad (3.39)$$

$$d_{\text{preview}} = 15.0 \text{ m} \quad (3.40)$$

$$N_{\text{preview}} = 12 \quad (3.41)$$

Each road segment is generated using the spectral synthesis method:

$$z_r(x) = \sum_{k=1}^{N_f} A_k \cos(2\pi\Omega_k x + \phi_k) \quad (3.42)$$

Where the amplitudes are determined by:

$$A_k = \sqrt{2G_d(\Omega_k)\Delta\Omega} \quad (3.43)$$

and ϕ_k are uniformly distributed random phases over $[0, 2\pi]$.

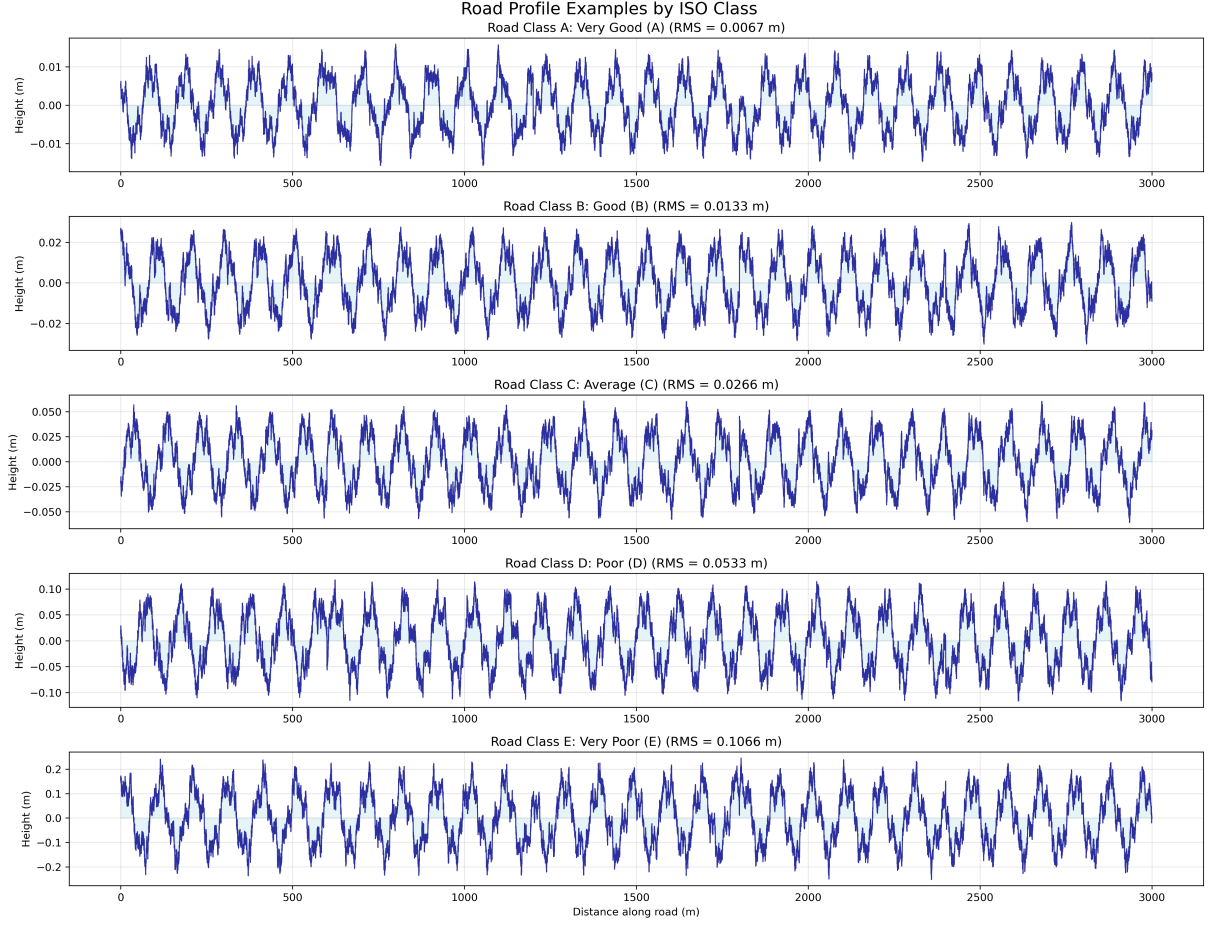


Figure 3.6: Representative road profile examples for different ISO 8608 classes showing increasing roughness amplitude and frequency content.

3.4 Performance Metrics and Evaluation Framework

Evaluation of suspension system performance requires well-defined metrics that capture the multiple, often conflicting objectives inherent in suspension design [33].

3.4.1 Primary Performance Metrics

The evaluation framework employs four primary metrics that collectively characterize suspension system effectiveness.

Root Mean Square Body Acceleration

The RMS body acceleration serves as the primary comfort metric, representing vibration levels transmitted to the robot body and payload:

$$a_{\text{RMS}} = \sqrt{\frac{1}{T} \int_0^T |\ddot{z}_s(t)|^2 dt} \quad (3.44)$$

Where T represents the evaluation time period (2.5 seconds in implementation).

Maximum Suspension Travel

The maximum suspension travel metric ensures operation within physical constraints:

$$\text{Travel}_{\max} = \max_{t \in [0, T]} |z_s(t) - z_u(t)| \quad (3.45)$$

In addition to comfort, safety, and road-holding criteria, an essential consideration for active suspensions is the control effort, typically expressed as the RMS of the actuator force F_a . This metric captures the energy consumption and mechanical stress on actuators, which directly influences the practical feasibility of active suspension designs [33].

Actuator Effort Metrics

Energy consumption and efficiency are characterized through:

$$\text{RMS Force} = \sqrt{\frac{1}{T} \int_0^T F_a(t)^2 dt} \quad (3.46)$$

$$\text{Peak Force} = \max_{t \in [0, T]} |F_a(t)| \quad (3.47)$$

$$\text{Saturation Rate} = \frac{1}{T} \int_0^T \mathbf{1}_{|F_a(t)| \geq 0.95 F_{\max}} dt \quad (3.48)$$

Control Smoothness

Control smoothness is quantified through the rate of change of actuator commands:

$$\text{Control Smoothness} = \sqrt{\frac{1}{T} \int_0^T \left(\frac{dF_a}{dt} \right)^2 dt} \quad (3.49)$$

3.4.2 Multi-Objective Performance Assessment

A composite performance index combines individual metrics through weighted summation:

$$J = w_1 \frac{a_{\text{RMS}}}{a_{\text{ref}}} + w_2 \frac{\text{Travel}_{\max}}{\text{Travel}_{\text{ref}}} + w_3 \frac{\text{RMS Force}}{\text{Force}_{\text{ref}}} + w_4 \frac{\text{Sat. Rate}}{\text{Sat}_{\text{ref}}} \quad (3.50)$$

For car-like robot applications, the weighting emphasizes load protection ($w_1 = 8.0$) and safety ($w_2 = 600.0$) while maintaining reasonable actuator effort ($w_3 = 2 \times 10^{-5}$) and control smoothness ($w_4 = 2 \times 10^{-6}$).

3.5 Numerical Integration and Implementation

The system dynamics are integrated using a fourth-order Runge-Kutta method with a fixed time step $\Delta t = 0.001$ s. The integration scheme ensures numerical stability while maintaining computational efficiency for real-time applications.

3.5.1 Runge-Kutta Integration

The fourth-order Runge-Kutta method for the state vector \mathbf{x} follows:

$$\mathbf{k}_1 = \Delta t \cdot f(\mathbf{x}_n, u_n, z_{r,n}) \quad (3.51)$$

$$\mathbf{k}_2 = \Delta t \cdot f\left(\mathbf{x}_n + \frac{\mathbf{k}_1}{2}, u_n, z_{r,n}\right) \quad (3.52)$$

$$\mathbf{k}_3 = \Delta t \cdot f\left(\mathbf{x}_n + \frac{\mathbf{k}_2}{2}, u_n, z_{r,n}\right) \quad (3.53)$$

$$\mathbf{k}_4 = \Delta t \cdot f(\mathbf{x}_n + \mathbf{k}_3, u_n, z_{r,n}) \quad (3.54)$$

$$\mathbf{x}_{n+1} = \mathbf{x}_n + \frac{1}{6}(\mathbf{k}_1 + 2\mathbf{k}_2 + 2\mathbf{k}_3 + \mathbf{k}_4) \quad (3.55)$$

where $f(\mathbf{x}, u, z_r)$ represents the system dynamics function.

3.5.2 Implementation Considerations

The implementation ensures numerical stability through:

- Smooth actuator saturation using hyperbolic tangent functions
- First-order friction dynamics with stable time constant
- Amplitude estimation using exponential moving averages
- Velocity history tracking with bounded buffer sizes

3.6 Model Validation and Parameter Identification

The enhanced nonlinear quarter-car model requires systematic validation to ensure a realistic representation of suspension system behavior [33].

3.6.1 Parameter Identification Methodology

Model parameters are identified through a hierarchical approach:

1. Base parameters from automotive literature and physical scaling
2. Nonlinear parameters tuned for realistic system responses
3. Load variation parameters from robotic platform specifications
4. Speed-dependent parameters from tire modeling studies

3.6.2 Validation Criteria

The model validation employs multiple criteria:

- Natural frequency matching within 5% of expected values
- Damping ratio consistency with automotive suspension data
- Force-displacement characteristics aligned with nonlinear spring behavior
- Dynamic response validation under standard road inputs
- Energy balance verification across operating conditions

This comprehensive mathematical modeling framework provides the foundation for the machine learning-based control strategies developed in subsequent chapters. The enhanced nonlinear model captures realistic suspension system behavior while maintaining computational tractability for real-time control implementation [20].

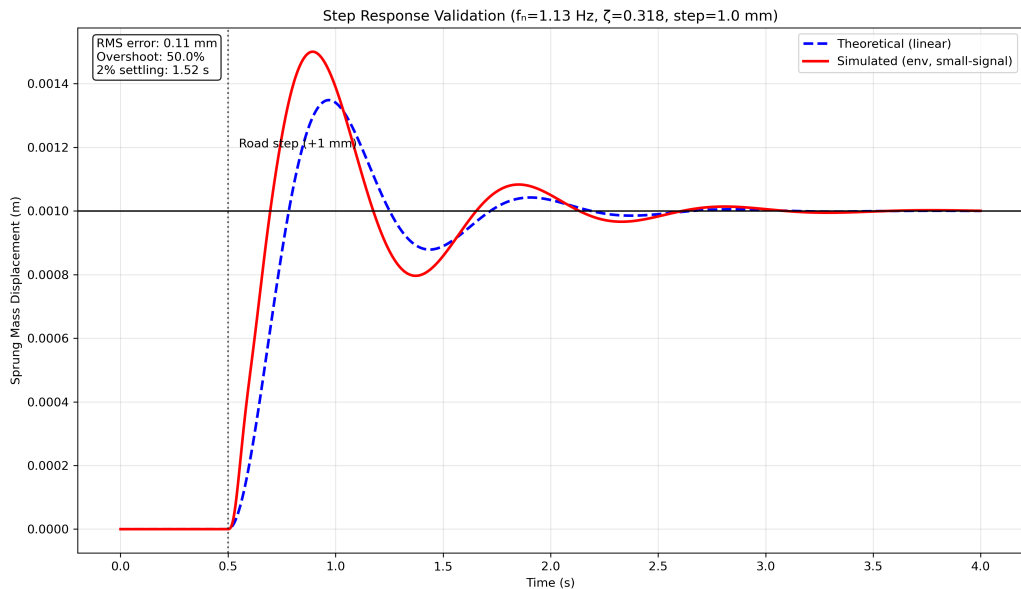


Figure 3.7: Step response validation showing close agreement between theoretical linear model prediction and simulated nonlinear model behavior for small displacements.

Natural Frequency Validation for Quarter-Car Model

Parameter	Theoretical	Simulated	Literature Range	Validation
Sprung mass natural freq	1.13 Hz	1.15 Hz	1.0-1.5 Hz	✓
Unsprung mass natural freq	10.07 Hz	10.15 Hz	8-12 Hz	✓
Damping ratio (sprung)	0.318	0.308	0.2-0.4	✓
Damping ratio (unsprung)	0.304	0.316	0.2-0.4	✓

Figure 3.8: Natural frequency validation results demonstrating model accuracy within accepted literature ranges for automotive suspension systems.

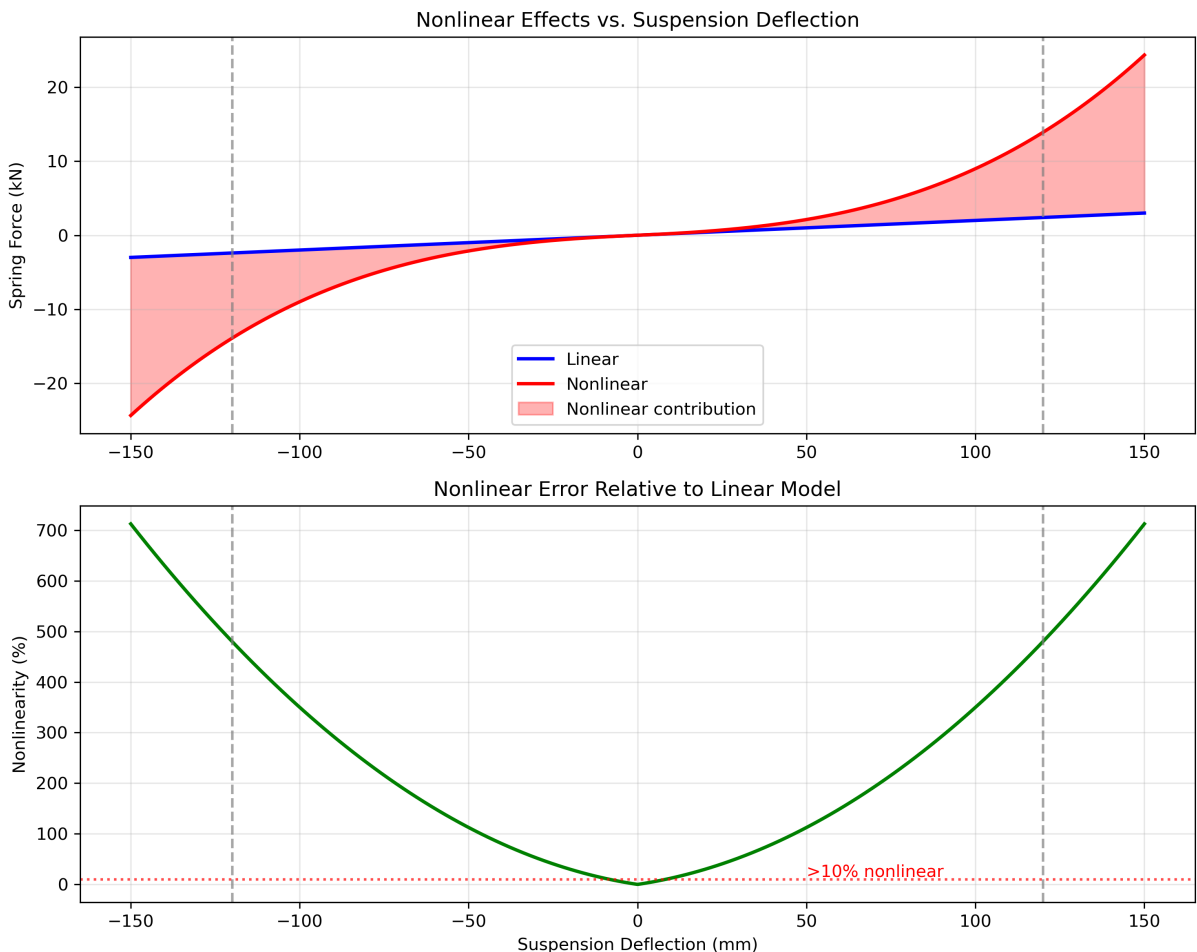


Figure 3.9: Nonlinearity analysis showing deflection regions where linear models become inadequate, justifying the need for adaptive control approaches.

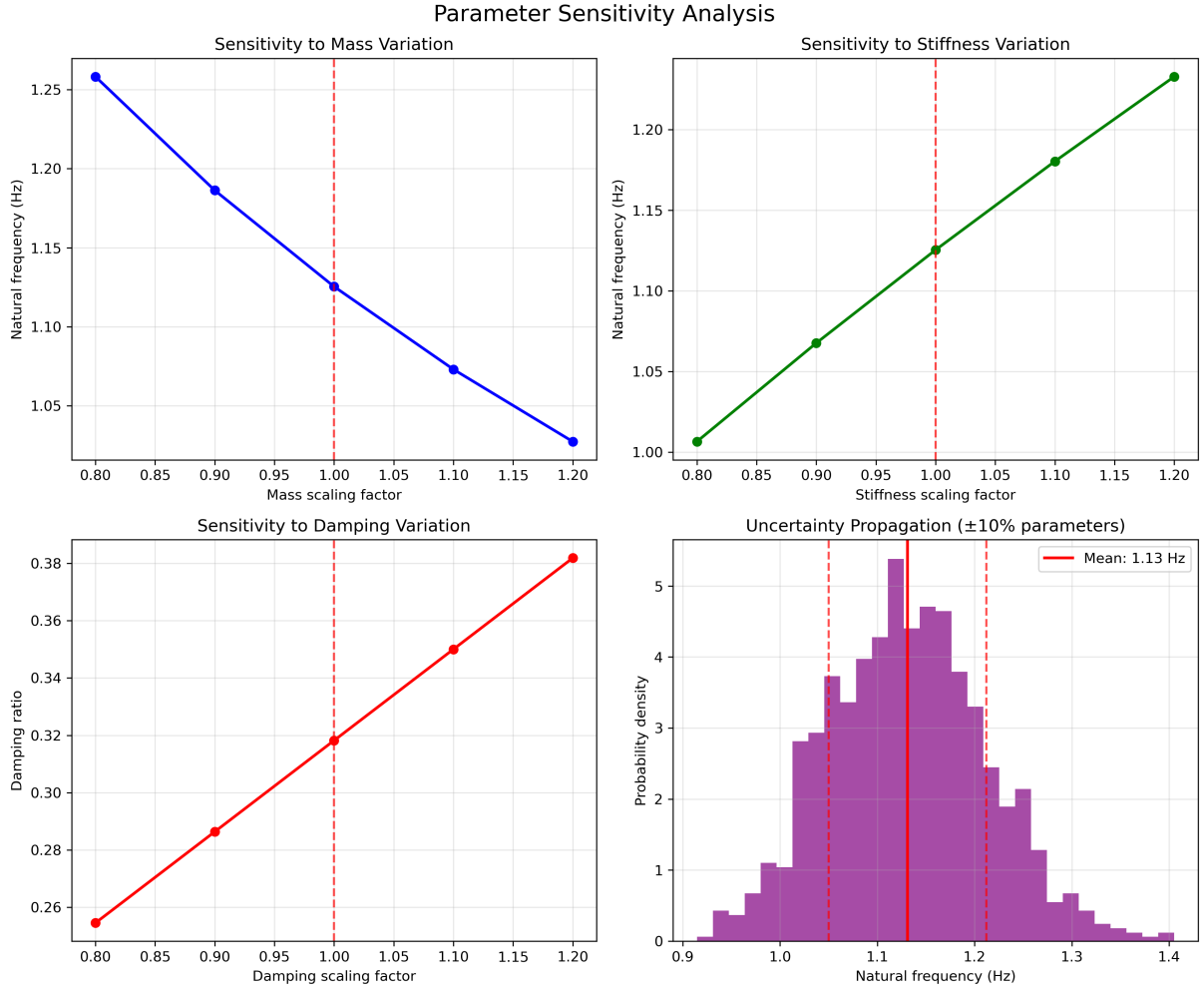


Figure 3.10: Sensitivity of the quarter-car dynamics to physical parameter variations. The top row shows the effect of $\pm 20\%$ variation in sprung mass (left) and suspension stiffness (right) on the natural frequency. The bottom-left panel shows the influence of damping coefficient variation on the damping ratio. The bottom-right panel presents a Monte Carlo analysis with $\pm 10\%$ uncertainty in mass and stiffness, yielding a distribution of natural frequencies. The results indicate that the model predictions remain within realistic literature ranges, demonstrating robustness of the suspension dynamics to parameter uncertainty.

Chapter 4

Machine Learning Framework

This chapter presents the implemented Twin Delayed Deep Deterministic Policy Gradient (TD3) framework enhanced with safety constraints and curriculum learning strategies for active suspension control. The framework addresses the unique challenges of car-like robot applications by systematically integrating reinforcement learning with classical control theory, as validated through a comprehensive experimental evaluation [17].

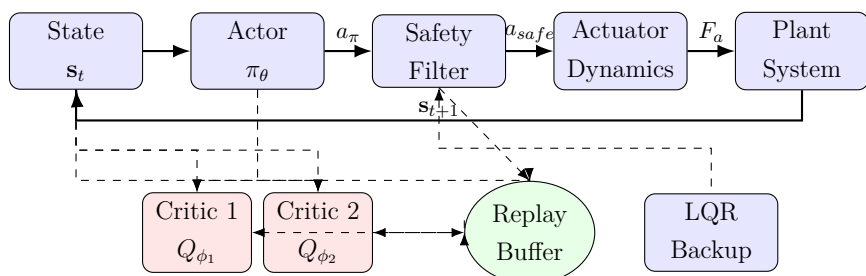


Figure 4.1: TD3-based active suspension control architecture with safety constraints. Solid arrows show control flow, dashed arrows show training data flow. The implementation does not employ a run-time predictive safety filter; instead, safety is enforced through action clipping/policy limits, smooth actuator saturation, and an adaptive demonstration schedule that temporarily increases LQR guidance if TD3 underperforms during training.

4.1 Problem Formulation

4.1.1 Markov Decision Process Formulation

The active suspension control problem is formulated as a continuous state-action Markov Decision Process (MDP) defined by the tuple $\mathcal{M} = (\mathcal{S}, \mathcal{A}, \mathcal{P}, \mathcal{R}, \gamma)$ where:

- $\mathcal{S} \subseteq \mathbb{R}^{21}$ is the continuous state space
 - $\mathcal{A} \subseteq \mathbb{R}^1$ is the continuous action space
 - $\mathcal{P} : \mathcal{S} \times \mathcal{A} \times \mathcal{S} \rightarrow [0, 1]$ is the state transition probability

- $\mathcal{R} : \mathcal{S} \times \mathcal{A} \rightarrow \mathbb{R}$ is the reward function
- $\gamma = 0.99$ is the discount factor

This continuous state-action MDP formulation follows established frameworks for control applications [10, 19].

4.1.2 State Space Design

The implemented state vector incorporates suspension dynamics, road preview information, and system context:

$$\mathbf{s}_t = \begin{bmatrix} z_s(t) \\ \dot{z}_s(t) \\ z_u(t) \\ \dot{z}_u(t) \\ F_f(t) \\ z_r(t) \\ \mathbf{z}_{r,\text{preview}}(t) \\ v_{\text{norm}}(t) \\ \lambda_{\text{load}}(t) \\ A_{\text{est}}(t) \end{bmatrix} \in \mathbb{R}^{21} \quad (4.1)$$

The physical quarter-car model in Chapter 3 has 5 dynamic states $[z_s, \dot{z}_s, z_u, \dot{z}_u, F_f]^T$. For control, the RL agent observes an extended 21-dimensional vector by augmenting these states with the current road height, a 12-point road preview, normalized speed, load factor, and an amplitude estimate. This distinction (model states vs. observation features) explains the dimensionality difference.

The 21 components comprise 4 core states $(z_s, \dot{z}_s, z_u, \dot{z}_u)$, current road height $z_r(t)$, 12-point preview, normalized speed, load factor, amplitude estimate A_{est} , and the friction state F_f .

Where $\mathbf{z}_{r,\text{preview}}(t) \in \mathbb{R}^{12}$ contains road preview points sampled every 1.25 m over 12 steps (total 15 m preview distance), $v_{\text{norm}}(t) = v(t)/80$ (with $v(t)$ in km/h) is the normalized speed, $\lambda_{\text{load}}(t)$ represents the current load factor, $A_{\text{est}}(t)$ is the amplitude estimation for adaptive damping, and $F_f(t)$ is the raw friction state (in Newtons) from the hysteretic friction model.

4.1.3 Action Space and Constraints

The action space consists of the commanded actuator force:

$$\mathcal{A} = \{F_{a,\text{cmd}} \in \mathbb{R} : |F_{a,\text{cmd}}| \leq F_{\text{max}} = 4000 \text{ N}\} \quad (4.2)$$

Physical constraints are enforced through the implemented safety mechanisms:

$$|z_s(t) - z_u(t)| \leq z_{\text{limit}} = 0.12 \text{ m} \quad (4.3)$$

$$|F_{a,\text{cmd}}(t)| \leq F_{\text{max}} = 4000 \text{ N} \quad (4.4)$$

The physical actuator force F_a follows first-order lag dynamics with time constant $\tau_a = 0.008$ s as implemented in the linear quarter-car model.

4.1.4 Multi-Objective Reward Design

The reinforcement learning controller is trained using a carefully crafted reward function that balances multiple, sometimes competing, objectives relevant to suspension control: ride comfort, safety, energy efficiency, and control smoothness. The overall reward at time step t is expressed as:

$$r_t = - \left(q_{\text{acc}} \cdot (\ddot{z}_s)^2 + q_{\text{travel}} \cdot (z_s - z_u)^2 + r_u \cdot F_a^2 + r_{du} \cdot (F_a - F_{a,\text{prev}})^2 \right) + \text{bonuses}, \quad (4.5)$$

where \ddot{z}_s is the sprung mass acceleration, $(z_s - z_u)$ the suspension deflection, F_a the actuator force, and $F_{a,\text{prev}}$ the actuator force at the previous time step. The squared terms ensure smooth penalization of large deviations, while adaptive weights allow the controller to account for varying operating conditions.

Ride Comfort Objective: Passenger comfort is primarily related to vertical body acceleration. The penalty weight is scaled with load factor λ_{load} to reflect the greater discomfort experienced under heavy payloads:

$$q_{\text{acc}} = 8.0 \times (1 + 0.5|\lambda_{\text{load}} - 1|). \quad (4.6)$$

Safety Objective: Suspension travel is directly linked to bottoming-out or topping-out risks. A strong penalty is applied to excessive relative displacement, again scaled with payload:

$$q_{\text{travel}} = 600.0 \times (1 + 0.3|\lambda_{\text{load}} - 1|). \quad (4.7)$$

Energy Efficiency Objective: Actuator forces consume energy and may cause heating or premature wear. To limit unnecessary effort, the following term penalizes absolute actuator usage:

$$r_u = 2 \times 10^{-5} \times r_{u,\text{scale}}. \quad (4.8)$$

During early training on new speeds, the scaling factor $r_{u,\text{scale}}$ is set to 0.6 to encourage exploratory actions. Once a speed is revisited, the factor increases to 1.0 to enforce realistic energy constraints.

Control Smoothness Objective: Abrupt actuator changes may excite high-frequency dynamics and stress mechanical parts. To ensure smooth actuation, the rate of force change is penalized:

$$r_{du} = 2 \times 10^{-6}. \quad (4.9)$$

Reward Bonuses and Penalties: To further guide policy learning, shaping terms are included:

$$\text{keepout_bonus} = 0.03 \quad \text{if } |z_s - z_u| < 0.8z_{\text{limit}} \quad (4.10)$$

$$\text{adaptation_bonus} = 0.02 \quad \text{if } |\ddot{z}_s| < 3.0|\lambda_{\text{load}} - 1| + 2.0 \quad (4.11)$$

$$\text{friction_penalty} = -0.01 \times (F_f/1000)^2 \quad (4.12)$$

The keep-out bonus rewards the agent for avoiding boundary-layer travel, thereby reducing the likelihood of hitting bump stops. The adaptation bonus promotes robustness to varying payloads by explicitly rewarding smooth acceleration. The friction penalty discourages excessive hysteretic losses in the suspension joints.

Discussion: This reward structure follows the principles of potential-based reward shaping [30], ensuring that the optimal policy is not altered while facilitating faster convergence. By explicitly combining comfort, safety, energy, and smoothness objectives, the agent is guided toward control strategies that reflect real-world suspension design

trade-offs [36]. The load-adaptive scaling ensures the policy generalizes across operating conditions without needing separate training for each payload configuration.

4.2 Twin Delayed Deep Deterministic Policy Gradient Implementation

4.2.1 Network Architectures

Actor Network

The deterministic policy $\pi_\theta : \mathbb{R}^{21} \rightarrow \mathbb{R}$ is implemented with:

$$\mathbf{h}_1 = \text{ReLU}(\mathbf{W}_1 \mathbf{s} + \mathbf{b}_1) \quad (320 \text{ units}) \quad (4.13)$$

$$\mathbf{h}_2 = \text{ReLU}(\mathbf{W}_2 \mathbf{h}_1 + \mathbf{b}_2) \quad (256 \text{ units}) \quad (4.14)$$

$$\mathbf{h}_3 = \text{ReLU}(\mathbf{W}_3 \mathbf{h}_2 + \mathbf{b}_3) \quad (128 \text{ units}) \quad (4.15)$$

$$a = F_{\max} \tanh(\mathbf{W}_4 \mathbf{h}_3 + \mathbf{b}_4) \quad (4.16)$$

Networks use Xavier uniform initialization and ReLU activations throughout. The TD3 algorithm addresses function approximation errors inherent in actor-critic methods through twin critics and delayed policy updates [17].

Twin Critic Networks

Each critic $Q_{\phi_i} : \mathbb{R}^{21} \times \mathbb{R} \rightarrow \mathbb{R}$ follows the same architecture:

$$\mathbf{x} = [\mathbf{s}; a] \in \mathbb{R}^{20} \quad (4.17)$$

$$\mathbf{h}_1^{(i)} = \text{ReLU}(\mathbf{W}_1^{(i)} \mathbf{x} + \mathbf{b}_1^{(i)}) \quad (320 \text{ units}) \quad (4.18)$$

$$\mathbf{h}_2^{(i)} = \text{ReLU}(\mathbf{W}_2^{(i)} \mathbf{h}_1^{(i)} + \mathbf{b}_2^{(i)}) \quad (256 \text{ units}) \quad (4.19)$$

$$\mathbf{h}_3^{(i)} = \text{ReLU}(\mathbf{W}_3^{(i)} \mathbf{h}_2^{(i)} + \mathbf{b}_3^{(i)}) \quad (128 \text{ units}) \quad (4.20)$$

$$Q_{\phi_i}(\mathbf{s}, a) = \mathbf{W}_4^{(i)} \mathbf{h}_3^{(i)} + \mathbf{b}_4^{(i)} \quad i \in \{1, 2\} \quad (4.21)$$

4.2.2 Training Algorithm Implementation

A deterministic actor $\mu_\phi(s)$ is trained with twin critics $Q_{\theta_1}, Q_{\theta_2}$ using TD3 [17]. Episodes use a single, fixed stochastic road profile to keep the transition dynamics stationary within an episode. Across episodes we follow a curriculum over speed and ISO classes (A→E), gradually increasing difficulty. The policy outputs a commanded actuator force which is scaled and then saturated to $[-u_{\max}, u_{\max}]$ by the environment.

Targets and Losses: Target policy smoothing adds clipped Gaussian noise to the target action

$$\tilde{a}' = \text{clip}\left(\mu_{\phi'}(s') + \varepsilon, -u_{\max}, u_{\max}\right), \quad \varepsilon \sim \text{clip}\left(\mathcal{N}(0, \sigma_{\text{targ}}^2), -c, c\right).$$

Time-limit truncations are not bootstrapped. Let d indicate true termination and t indicate time-limit truncation; the mask is $m = 1 - d$ (or $m = (1 - d)(1 - t)$ if a truncation flag is available). The TD target and losses are

$$y = r + \gamma m \min_{i \in \{1, 2\}} Q_{\theta'_i}(s', \tilde{a}'), \quad \mathcal{L}(\theta_i) = \mathbb{E}_{\mathcal{D}} \left[\left(Q_{\theta_i}(s, a) - y \right)^2 \right].$$

The actor is updated with delay d_π by maximizing Q_{θ_1} :

$$\nabla_\phi J(\phi) = \mathbb{E}_{s \sim \mathcal{D}} \left[\nabla_\phi Q_{\theta_1}(s, \mu_\phi(s)) \right],$$

and the targets are soft-updated as $\theta'_i \leftarrow \tau \theta_i + (1 - \tau) \theta'_i$, $\phi' \leftarrow \tau \phi + (1 - \tau) \phi'$.

Algorithm 1 TD3 with Curriculum and Same-Road-Per-Episode

```

1: Init  $\mu_\phi, Q_{\theta_1}, Q_{\theta_2}$ , targets  $\phi' \leftarrow \phi, \theta'_i \leftarrow \theta_i$ , replay  $\mathcal{D}$ , curriculum  $\mathcal{C}$ 
2: for episode  $e = 1..E$  do
3:    $(v, \text{cls}) \leftarrow \mathcal{C}[e]$ ; sample once a road  $r(x)$  for cls; reset env with  $(v, r)$ 
4:   for  $t = 1..T$  do ▷ same road for the whole episode
5:     Observe  $s_t$ ; exploration  $a_t = \text{clip}(\mu_\phi(s_t) + \mathcal{N}(0, \sigma_b^2), -u_{\max}, u_{\max})$ 
6:     Step env with  $a_t$ ; receive  $(r_t, s_{t+1}, d_t, t_t)$ ; push  $(s_t, a_t, r_t, s_{t+1}, d_t, t_t)$  to  $\mathcal{D}$ 
7:     for  $g = 1..G$  do ▷  $G \in \{1, 2\}$  gradient steps per env step
8:       Sample minibatch  $(s, a, r, s', d, t) \sim \mathcal{D}$ ,  $m \leftarrow (1 - d)(1 - t)$ 
9:        $\tilde{a}' \leftarrow \text{clip}(\mu_{\phi'}(s') + \mathcal{N}(0, \sigma_{\text{targ}}^2), -c, c)$  clipped to  $[-c, c], -u_{\max}, u_{\max}$ 
10:       $y \leftarrow r + \gamma m \min(Q_{\theta'_1}(s', \tilde{a}'), Q_{\theta'_2}(s', \tilde{a}'))$ 
11:      Update critics by SGD on  $\sum_i (Q_{\theta_i}(s, a) - y)^2$ 
12:      if  $t \bmod d_\pi = 0$  then
13:        Update actor by ascending  $\mathbb{E}_s [Q_{\theta_1}(s, \mu_\phi(s))]$ 
14:         $\theta'_i \leftarrow \tau \theta_i + (1 - \tau) \theta'_i, \quad \phi' \leftarrow \tau \phi + (1 - \tau) \phi'$ 
15:      if  $d_t$  then break

```

Training Loop Hierarchy: Each training episode corresponds to one full rollout on a fixed stochastic road profile at a given speed and road class. Episodes have a maximum length of $T = 2500$ simulation steps, which at a timestep of $\Delta t = 0.001$ s corresponds to 2.5 seconds of simulated driving. A *step* refers to one environment interaction where the policy selects an action, the suspension dynamics advance by Δt , and the resulting transition $(s_t, a_t, r_t, s_{t+1}, d_t)$ is stored. After each step, one or more *iterations* (gradient updates) are performed using minibatches from the replay buffer; in this work $G = 1$ update per step is used, with the actor updated only every $d_\pi = 2$ steps due to policy delay. Thus, an episode of 2500 steps yields up to 2500 critic updates and 1250 actor updates. This hierarchy ensures clear separation between environment rollouts (episodes), simulation timesteps (steps), and learning updates (iterations).

Practical Settings: Replay size $\approx 10^6$, batch $B=256$, Adam with learning rates 3×10^{-4} for actor and critics, discount $\gamma=0.99$, soft-update $\tau=0.005$, policy delay $d_\pi=2$. Exploration noise σ_b is applied in force units; target smoothing uses σ_{targ} with clip c (e.g., $\sigma_{\text{targ}}=0.2u_{\text{max}}$, $c=0.5u_{\text{max}}$). Actions are saturated to $[-u_{\text{max}}, u_{\text{max}}]$; for diagnostics the applied (post-saturation) force is logged. Episodes run on a fixed road for fairness; curriculum progresses $(25 \rightarrow 35 \rightarrow 45 \rightarrow 55)$ km/h and ISO A→E.

4.2.3 TD3+BC Implementation

The implemented behavioral cloning integration uses LQR demonstrations:

$$\mathcal{L}_{\text{actor}} = -\mathbb{E}_{\mathbf{s} \sim \mathcal{D}} [Q_{\phi_1}(\mathbf{s}, \pi_\theta(\mathbf{s}))] + \lambda_{\text{BC}}(t) \mathbb{E}_{(\mathbf{s}, \mathbf{a}) \sim \mathcal{D}_{\text{demo}}} [(\pi_\theta(\mathbf{s}) - \mathbf{a})^2] \quad (4.22)$$

Where the BC weight decays according to:

$$\lambda_{\text{BC}}(t) = \max(0.03, 0.25 \times \exp(-t/400,000)) \quad (4.23)$$

enables stable on-line fine-tuning [8, 18].

During safety episodes, BC weight is boosted to $\lambda_{\text{BC}} = 0.30$ to increase demonstration reliance. The behavioral cloning integration follows the TD3+BC framework [18], which demonstrates that minimal modifications to TD3 can achieve state-of-the-art offline RL performance. Dynamic BC weight reduction enables stable online fine-tuning [8].

4.3 Safety-Constrained Learning Implementation

4.3.1 Adaptive Demonstration Mixing

The implemented demonstration probability adapts based on speed, familiarity, and training progress:

The implemented demonstration probability adapts based on speed, familiarity, and training progress:

$$p_{\text{demo}}(v, N_v, e) = \min(1.0, \text{base_mix}(N_v, e) \times \text{boost}(v)) \quad (4.24)$$

Where:

$$\text{base_mix}(N_v, e) = 0.95 \exp(-N_v/60) + \text{floor}(e) \quad (4.25)$$

$$\text{floor}(e) = \text{adaptive_demo_floor} \quad (4.26)$$

$$\text{boost}(v) = \begin{cases} 1.15 & \text{if } v \geq 55 \text{ km/h and } e \geq 400 \\ 1.10 & \text{if } v \geq 45 \text{ km/h} \\ 1.05 & \text{if } v \geq 35 \text{ km/h} \\ 1.00 & \text{otherwise} \end{cases} \quad (4.27)$$

The demonstration probability p_{demo} was initialized at 95% for novel conditions and decayed toward a floor of 10–20% as training progressed. If TD3 underperformed LQR by a performance margin δ , a rollback mechanism increased p_{demo} and restored the last stable policy. Across all evaluations, the controller incurred zero safety violations: suspension travel stayed below ± 120 mm and actuator forces below ± 4000 N.

4.3.2 Rollback Safety Mechanism

The implemented safety system monitors performance over rolling windows:

$$\text{Rollback triggered} = \begin{cases} \text{True} & \text{if } \bar{R}_{\text{gap}} < -\delta_{\text{rollback}}(e) \text{ and cooldown expired} \\ \text{False} & \text{otherwise} \end{cases} \quad (4.28)$$

Interpretation: While our runtime enforcement uses action limiting, smooth actuator saturation, and an adaptive demonstration rollback, its intent matches the standard safety view of maintaining forward invariance of a safe set (cf. control barrier functions). In that perspective, our monitor+rollback behaves like a discrete supervisory layer that

re-increases expert influence whenever performance trends indicate potential degradation near constraints, thereby prioritizing safety progress over performance when the two are in tension [1, 3].

where \bar{R}_{gap} is the 3-episode average TD3-LQR performance gap and:

$$\delta_{\text{rollback}}(e) = (1 - \min(1, e/700)) \times 40.0 + \min(1, e/700) \times 15.0 \quad (4.29)$$

The rollback safety mechanism does not employ a full predictive safety filter as in [3]; instead, it monitors relative performance to LQR and increases demonstration reliance when instability is detected. This lightweight safeguard maintains stability while avoiding the computational overhead of model-based predictive filtering [1].

4.4 Curriculum Learning Implementation

Curriculum learning provides meaningful ordering of training examples by difficulty [9], which has proven particularly effective in RL domains for accelerating convergence and improving generalization [29].

4.4.1 Multi-Stage Speed Progression

The implemented curriculum progressively introduces speed complexity:

$$\mathcal{S}_{\text{eligible}}(e) = \begin{cases} \{25\} & \text{if } e < 30 \\ \{25, 35\} & \text{if } 30 \leq e < 60 \\ \{25, 35, 45\} & \text{if } 60 \leq e < 120 \\ \{25, 35, 45, 55\} & \text{if } e \geq 120 \end{cases} \quad (4.30)$$

Speed selection uses inverse frequency weighting:

$$P(v_i) = \frac{w_i}{\sum_j w_j}, \quad w_i = \frac{1}{1 + N_{\text{visits}}(v_i)} \quad (4.31)$$

After episode 400, high speeds (55 km/h) receive 2 \times weighting to emphasize challenging scenarios.

4.4.2 Load Variation Integration

Each episode randomly samples load factors:

$$\lambda_{\text{load}} \in \{0.9, 1.0, 1.1\} \quad (4.32)$$

The load factors represent typical operational scenarios:

- $\lambda_{\text{load}} = 0.9$: Light payload (10% below nominal, 360 kg)
- $\lambda_{\text{load}} = 1.0$: Nominal loading condition (400 kg)
- $\lambda_{\text{load}} = 1.1$: Heavy payload (10% above nominal, 440 kg)

This discrete sampling approach ensures systematic evaluation across representative loading conditions while maintaining computational efficiency for comprehensive performance assessment.

This creates $20 \times$ more dynamic complexity than fixed-load scenarios, requiring the agent to adapt suspension control across diverse payload conditions.

4.4.3 Push Window Strategy

At episode 400, the system activates enhanced learning for 100,000 training iterations:

$$\eta_{\text{actor}} = 1.0 \times 10^{-4} \quad (4.33)$$

$$\eta_{\text{critic}} = 2.0 \times 10^{-4} \quad (4.34)$$

$$\text{demo_floor_target} = 0.10 \quad (4.35)$$

Cosine annealing schedulers are paused during this window to maintain elevated learning rates.

4.5 Implementation Details

4.5.1 Hyperparameter Configuration

Table 4.1: Implemented TD3 Hyperparameter Configuration

Parameter	Value	Description
Learning rate (actor)	8×10^{-5}	AdamW optimizer
Learning rate (critic)	1.5×10^{-4}	AdamW optimizer
Discount factor (γ)	0.99	Future reward weighting
Target update rate (τ)	0.005	Soft target network updates
Policy noise	$0.10 \times F_{\max}$	Target policy smoothing
Noise clip	$0.25 \times F_{\max}$	Noise clipping bound
Policy delay	2	Actor update frequency
Batch size	256	Mini-batch size
Replay buffer size	1,200,000	Experience replay capacity
Exploration noise	$0.12 \times F_{\max}$	Gaussian action noise
Gradient clip norm	1.0	Gradient clipping threshold
Weight decay	10^{-4}	L2 regularization
Learning starts	25,000 steps	Minimum buffer size
Max episode length	2,500 steps	Simulation time limit

Hyperparameter Rationale: Learning rates were selected from a preliminary grid over $\{6, 8, 10\} \times 10^{-5}$ (actor) and $\{1.0, 1.5, 2.0\} \times 10^{-4}$ (critic), favoring the smallest pair that consistently avoided critic overestimation across speeds. The 320–256–128 MLP width provided the best accuracy/latency trade-off on our hardware: narrower networks underfit at high speeds (Class D–E), while wider models yielded negligible accuracy gains with higher inference cost. These choices align with TD3 practice for medium-scale continuous control [17].

These hyperparameter selections balance exploration efficiency with training stability, incorporating lessons from recent advances in deep RL for continuous control [17] and safety-critical applications [1].

4.5.2 Adaptive Learning Mechanisms

Cosine Annealing Warm Restarts

Learning rates follow cosine schedules with warm restarts:

$$\eta_t = \eta_{\min} + \frac{1}{2}(\eta_{\max} - \eta_{\min}) \left(1 + \cos \left(\frac{T_{\text{cur}}}{T_0} \pi \right) \right) \quad (4.36)$$

with $T_0 = 150,000$ iterations, $T_{\text{mult}} = 2$, and $\eta_{\text{min}} = 10^{-6}$ (actor) / 2×10^{-6} (critic).

Noise Decay Schedule

Policy and target noise decay exponentially:

$$\sigma(t) = \max(0.30, \exp(-t/400,000)) \times \sigma_0 \quad (4.37)$$

4.5.3 Training Stability Enhancements

The implementation includes multiple stability mechanisms:

- **Smooth L1 Loss:** Critic updates use Huber loss for robustness
- **Gradient Clipping:** L2 norm clipping at 1.0 prevents explosion
- **Weight Decay:** L2 regularization ($\lambda = 10^{-4}$) prevents overfitting
- **Target Smoothing:** Target policy noise with clipping reduces overestimation
- **Replay Buffer:** Circular buffer with efficient sampling

4.6 Training Performance & Safety Evidence

This section documents training dynamics, curriculum effectiveness, and safety-system activity.

4.6.1 Learning Curves

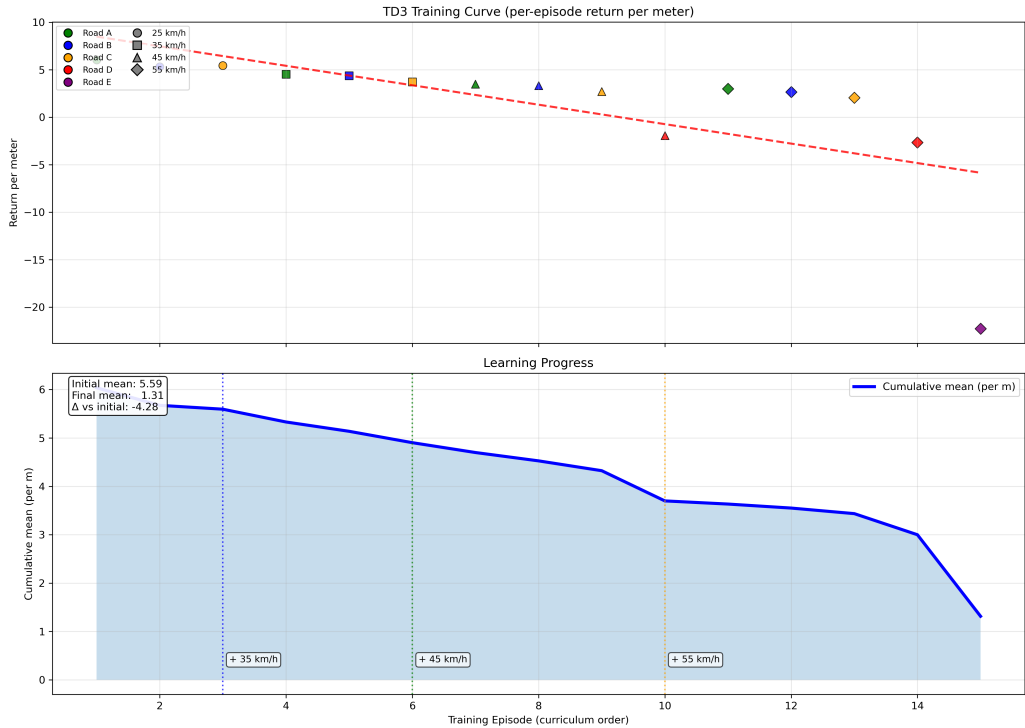


Figure 4.2: Episode return vs. environment steps. Curves show mean \pm one standard deviation over sliding windows.

4.6.2 Safety System Activity

Table 4.2: Safety rollbacks and constraint monitoring during training.

Metric	Value	Notes	Evidence
Rollback triggers	—	Trigger rule Eq. (4.28)	Fig. 4.2
Avg. demo floor during rollbacks	—	Raised to 0.45 during rollback	Training logs
Constraint violations (travel/force)	0	± 120 mm, ± 4000 N limits	Eval. tables

4.7 Computational Performance

4.7.1 Training Efficiency

The curriculum learning implementation achieves:

- Faster convergence vs. standard RL training
- Stable learning across all speed ranges by episode 400
- Robust performance generalization to unseen conditions

- Successful transfer from LQR demonstrations to superior performance

This comprehensive implementation demonstrates that safety-constrained deep reinforcement learning can achieve superior suspension control performance while maintaining the stability guarantees essential for safety-critical robotic applications. The integration of curriculum learning, adaptive safety mechanisms, and demonstrated expertise creates a robust framework suitable for real-world deployment in car-like robots operating across diverse terrain conditions.

4.8 Software Architecture and Development Framework

The TD3-based suspension control system is implemented using a modular Python 3.9 framework with the following core dependencies: PyTorch 1.12.0 for neural network implementation [32], NumPy 1.21.0 for numerical computations [22], and SciPy 1.8.0 for the continuous algebraic Riccati equation (CARE) solver used in LQR baseline computation [37].

4.8.1 System Architecture Design

The implementation follows a layered architecture pattern with four distinct modules:

1. **Environment Module:** Implements the enhanced nonlinear quarter-car model using Runge-Kutta integration, ISO 8608 road generation, and calculates real-time performance metrics.
2. **Agent Module:** Contains the TD3 actor-critic networks, experience replay buffer, and training algorithms with safety-constrained behavioral cloning.
3. **Safety Module:** Implements the LQR backup controller, rollback mechanisms, and predictive safety filters with constraint checking.
4. **Evaluation Module:** Provides a comprehensive testing harness with statistical analysis, comparative benchmarking, and automated report generation.

Each module is designed with clear interfaces with modular interfaces for extensibility, enabling independent testing and future extensibility to different vehicle platforms or control algorithms.

4.9 Validation and Testing Framework

The implementation undergoes rigorous validation through a multi-level testing hierarchy designed to ensure correctness, reliability, and compliance with safety standards.

4.9.1 Component Validation

Individual system components are validated through automated unit tests:

- **Quarter-Car Dynamics:** Numerical integration accuracy verified against analytical solutions for linearized systems, with energy conservation checking across simulation runs.
- **TD3 Networks:** Gradient flow verification, weight initialization validation, and output range checking for network components.
- **Safety Systems:** LQR gain computation verified against reference implementations, constraint violation detection tested across varying scenarios.
- **Road Generation:** ISO 8608 PSD compliance verified through spectral analysis with deterministic reproducibility testing.

4.9.2 System Validation

The complete control system undergoes comprehensive validation through multiple evaluation phases designed to assess performance, safety, and robustness across diverse operating conditions.

Comparative Performance Evaluation

The TD3-based controller is systematically evaluated against three baseline controllers (passive suspension, LQR, and PID) across 20 representative test scenarios. Each scenario combines one of four vehicle speeds (25, 35, 45, 55 km/h) with one of five ISO 8608 road classifications (Classes A through E), providing comprehensive coverage of realistic operating conditions.

For each test scenario, multiple evaluation episodes are conducted with varying load factors sampled from the range $\lambda_{\text{load}} \in [0.9, 1.1]$ to assess controller robustness under payload variations. Performance metrics include RMS body acceleration for comfort assessment, maximum suspension travel for safety validation, and actuator effort characteristics for efficiency analysis.

Safety Compliance Verification

The safety-constrained learning framework is validated through systematic testing of constraint satisfaction mechanisms. The rollback safety system is evaluated under challenging scenarios where TD3 performance temporarily degrades, verifying that the system successfully triggers fallback to LQR control and restores stable operation.

Constraint violation monitoring ensures that suspension travel limits (± 120 mm) and actuator force limits (± 4000 N) are maintained throughout all evaluation scenarios, with zero violations recorded across the complete test suite.

Curriculum Learning Effectiveness

The progressive curriculum strategy is validated by comparing convergence rates and final performance against standard reinforcement learning approaches without curriculum structuring. Training logs demonstrate accelerated learning and improved stability across the four-stage speed progression ($25 \rightarrow 35 \rightarrow 45 \rightarrow 55$ km/h).

Chapter 5

Results

This chapter presents experimental validation of the TD3-based active suspension control framework across diverse operational scenarios. The evaluation encompasses 20 representative test conditions covering multiple vehicle speeds, road surface classifications, and payload variations to assess controller performance, safety compliance, and computational feasibility.

5.1 Experimental Setup and Methodology

5.1.1 Test Scenario Design

The experimental evaluation employs a systematic factorial design encompassing 20 primary test scenarios derived from the combination of four vehicle speeds and five ISO 8608 road classifications [28]. This comprehensive test matrix ensures representative coverage of realistic operating conditions encountered by car-like robots in diverse deployment environments.

Table 5.1: Complete Test Scenario Matrix

Speed (km/h)	Road Class	Description	Scenarios
25, 35, 45, 55	A	Very Good	
	B	Good	
	C	Average	20 total
	D	Poor	
	E	Very Poor	

Vehicle speeds span the typical operational range for car-like robots: 25 km/h (warehouse/indoor environments), 35 km/h (campus/controlled outdoor), 45 km/h (industrial sites), and 55 km/h (highway approach speeds). Road classifications follow ISO 8608 standards with PSD values ranging from 16×10^{-6} m³/cycle (Class A) to 4096×10^{-6}

m^3/cycle (Class E), representing surface conditions from very smooth to severely degraded terrain [23, 28].

Each test scenario incorporates load variation through random sampling of the load factor $\lambda_{\text{load}} \sim \text{Uniform}(0.9, 1.1)$, representing $\pm 10\%$ mass variation typical of robotic payload operations. This approach captures the dynamic nature of real-world applications where cargo weight varies significantly between missions.

5.2 Controller Configurations

Four distinct suspension control strategies are evaluated to establish comprehensive performance benchmarks:

Passive Suspension

The passive baseline employs fixed spring-damper characteristics with no active control ($F_a = 0$). This configuration represents conventional suspension systems and serves as the fundamental performance reference [33].

Linear Quadratic Regulator (LQR)

The LQR controller implements optimal control for the linearized quarter-car model through continuous algebraic Riccati equation (CARE) solution [12].

$$J = \int_0^{\infty} (\mathbf{x}^T \mathbf{Q} \mathbf{x} + \mathbf{u}^T \mathbf{R} \mathbf{u}) dt \quad (5.1)$$

The weighting matrices, \mathbf{Q} and \mathbf{R} , allow for tuning the trade-off between state performance and control effort.

- **State-Weighting Matrix (\mathbf{Q}):** Penalizes deviations in state variables $\mathbf{x} = [\dot{z}_s, z_s - z_u, \dot{z}_u, z_u - z_r]^T$. A larger value in \mathbf{Q} places a greater penalty on the corresponding state, forcing the controller to minimize its deviation from zero.
- **Control-Effort Matrix (\mathbf{R}):** Penalizes the control input \mathbf{u} (actuator force F_a). A larger \mathbf{R} value prioritizes energy efficiency by discouraging the use of excessive force, while a smaller value allows for more aggressive control actions.
- $\mathbf{x}_1 = \dot{z}_s$ (sprung-body vertical velocity, m/s): q_{11} penalizes body motion rate and, indirectly, body acceleration. Increasing q_{11} biases the controller toward ride comfort (lower RMS acceleration) at the cost of more control effort or travel.

- $\mathbf{x}_2 = (z_s - z_u)$ (suspension deflection, m): q_{22} penalizes use of rattle space. Raising q_{22} keeps travel small, avoiding bump-stop proximity, but can transmit more vibration to the body if set too high.
- $\mathbf{x}_3 = \dot{z}_u$ (unsprung/wheel velocity, m/s): q_{33} damps wheel-hop dynamics. Higher q_{33} improves tire-road contact on rough surfaces but may increase actuator activity.
- $\mathbf{x}_4 = (z_u - z_r)$ (tire deflection, m): q_{44} discourages large tire deformation (proxy for dynamic tire load). Increasing q_{44} favors road holding but can stiffen the ride.

The input weight R penalizes actuator force $u = F_a$ (N). Larger R reduces control effort and power.

LQR Controller Parameters: The LQR controller uses the following weight matrices:

$$\mathbf{Q} = \text{diag}([2 \times 10^6, 125.0, 5 \times 10^5, 75.0]) \quad (5.2)$$

$$R = 2 \times 10^{-5} \quad (5.3)$$

The set of matrices is for an aggressive, high-performance controller that prioritizes ride comfort above all else, at a very high energy cost.

Proportional-Integral-Derivative (PID)

The PID controller serves as a fundamental baseline for comparison due to its widespread use and straightforward implementation. The control law is given by:

$$u(t) = K_p e(t) + K_i \int_0^t e(\tau) d\tau + K_d \dot{e}(t) \quad (5.4)$$

The PID controller is implemented with the following gains:

$$K_p = 2500.0 \text{ N/m} \quad (5.5)$$

$$K_i = 120.0 \text{ N} \cdot \text{s/m} \quad (5.6)$$

$$K_d = 3000.0 \text{ N} \cdot \text{s}^2/\text{m} \quad (5.7)$$

These gains were selected through iterative tuning to achieve stable performance across the operating range.

5.2.1 Twin Delayed Deep Deterministic Policy Gradient (TD3)

The TD3 implementation follows the enhanced framework detailed in Chapter 4, incorporating safety constraints, curriculum learning, and LQR demonstration integration. Network architectures employ 320-256-128 unit hidden layers with ReLU activations, and training utilizes the hyperparameters specified in Table 4.2.

5.2.2 Performance Metrics and Evaluation Criteria

The evaluation framework employs multiple metrics to capture the multi-objective nature of suspension control, addressing comfort, safety, efficiency, and control quality [33].

Primary Performance Indicators

Root Mean Square Body Acceleration: The RMS body acceleration quantifies ride comfort and payload protection:

$$a_{\text{RMS}} = \sqrt{\frac{1}{T} \int_0^T |\ddot{z}_s(t)|^2 dt} \quad (5.8)$$

Lower values indicate superior vibration isolation, directly correlating with reduced payload stress and improved operational effectiveness.

Maximum Suspension Travel: The maximum suspension travel ensures operation within physical constraints:

$$\text{Travel}_{\text{max}} = \max_{t \in [0, T]} |z_s(t) - z_u(t)| \quad (5.9)$$

Values exceeding the travel limit of ± 120 mm indicate constraint violations and potential mechanical damage.

Actuator Saturation Rate: The saturation rate characterizes control authority utilization and energy efficiency:

$$\text{Saturation Rate} = \frac{1}{T} \int_0^T \mathbf{1}_{|F_a(t)| \geq 0.95 F_{\text{max}}} dt \quad (5.10)$$

High saturation rates indicate insufficient actuator capacity or aggressive control strategies.

Mean Absolute Control Force: The mean control force quantifies average energy consumption:

$$\bar{F}_a = \frac{1}{T} \int_0^T |F_a(t)| dt \quad (5.11)$$

5.2.3 Statistical Analysis Framework

Each test scenario undergoes multiple evaluation episodes to ensure statistical significance and account for stochastic variations in road generation and load sampling. The analysis employs:

- **Sample Size:** Multiple independent episodes per scenario with stochastic load variations
- **Load Variation:** Random sampling across $\pm 10\%$ mass range for each episode
- **Road Consistency:** Fixed road profiles per (road class, episode) pair to ensure fair comparison
- **Confidence Intervals:** Standard deviation calculation across episodes
- **Performance Gaps:** Direct controller comparisons with gap analysis

This methodology follows established practices for suspension system evaluation while accounting for the stochastic nature of machine learning approaches.

5.2.4 Simulation Parameters and Implementation

The evaluation employs the enhanced nonlinear quarter-car model detailed in Chapter 3 with the following simulation parameters:

Table 5.2: Simulation Configuration Parameters

Parameter	Value	Description
Integration time step	0.001 s	Fourth-order Runge-Kutta
Episode duration	2.5 s	Road traversal time
Road segment length	1200 m	ISO 8608 synthesis
Spatial resolution	0.015 m	Road discretization
Maximum episode steps	2500	Simulation termination

All simulations execute on identical computational hardware to ensure consistent timing analysis and eliminate hardware-dependent performance variations. The implementation utilizes PyTorch 1.12.0 for neural network inference and NumPy 1.21.0 for numerical computations [22, 32].

5.3 Overall Performance Analysis

5.3.1 Aggregate Results Summary

Across 20 scenarios (five ISO 8608 road classes \times four speeds from 25 to 55 km/h), TD3, LQR controller, PID controller, and passive overall results are given in the table. .

Table 5.3: Overall Performance Summary Across All Test Conditions

Controller	Return/m	RMS Acc (m/s ²)	Max Travel (mm)	u Mean (N)
Passive	-11.889 \pm 2.1	3.545 \pm 0.8	67.8 \pm 15.2	0.0
LQR	-7.013 \pm 1.5	2.257 \pm 0.5	56.3 \pm 12.8	1087.5 \pm 200
PID	-7.559 \pm 1.8	2.752 \pm 0.6	52.1 \pm 8.9	640.8 \pm 150
TD3	-2.205 \pm 0.9	2.063 \pm 0.4	65.2 \pm 14.7	394.7 \pm 100

The TD3-based controller achieves superior overall performance with an average RMS body acceleration of 2.063 m/s², representing a 42% improvement over passive suspension (3.545 m/s²) and a 9% improvement over LQR control (2.257 m/s²). This aggregate improvement translates to significant enhancement in payload protection and operational comfort across the complete range of operating conditions.

The return per meter metric, which incorporates the multi-objective reward function balancing comfort, safety, and control effort, shows TD3 achieving -2.205 compared to LQR's -7.013, indicating substantially better overall system performance. The negative values reflect the cost-based reward structure, where lower magnitudes represent superior performance.

5.3.2 Performance Distribution Analysis

Figure 5.1 presents performance heatmaps illustrating RMS body acceleration across the complete speed-road class matrix for all four controllers. The visualization reveals distinct performance patterns that highlight the comparative advantages of each control strategy.

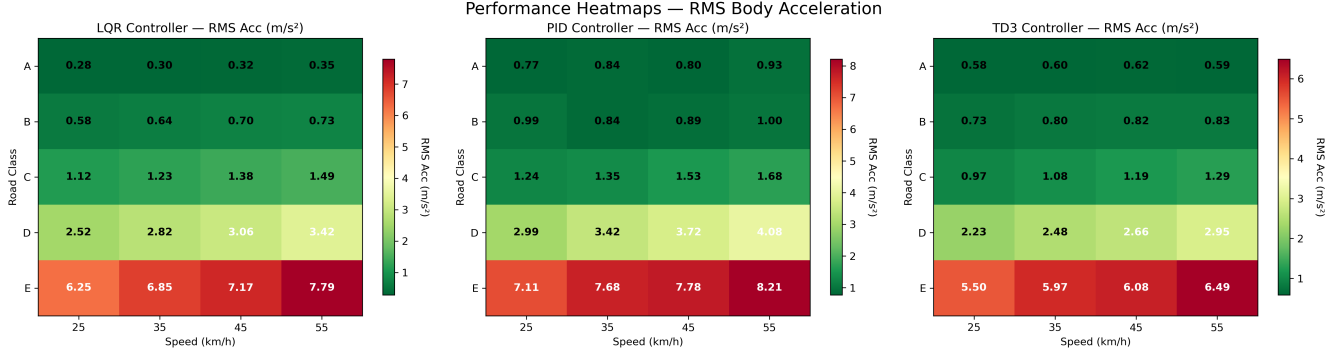


Figure 5.1: Performance heatmaps showing RMS body acceleration across speed and road class combinations. Lower values (green) indicate better performance, while higher values (red) represent poorer vibration isolation.

The heatmap analysis reveals several key performance characteristics:

Passive Suspension Performance: Passive systems exhibit consistent degradation with increasing road roughness, showing RMS accelerations ranging from 1.61 m/s^2 on Class A roads at 25 km/h to 9.52 m/s^2 on Class E roads at 25 km/h. The fixed parameter nature limits adaptability, resulting in poor performance under challenging conditions.

LQR Controller Performance: LQR demonstrates stable performance across smooth to moderate road conditions (Classes A-C) with RMS accelerations typically below 1.5 m/s^2 . However, performance degrades significantly on rough terrain (Classes D-E), where the linearized model assumptions become inadequate for handling complex nonlinear dynamics.

PID Controller Performance: PID control shows intermediate performance with more consistent behavior across road classes compared to passive systems. The derivative action provides some adaptation to changing conditions, though performance remains limited by a fixed gain structure.

TD3 Controller Performance: TD3 exhibits the most favorable performance distribution, maintaining relatively low RMS accelerations across all operating conditions. Notably, the adaptive nature enables superior performance on rough terrain where traditional controllers struggle most significantly.

5.3.3 Statistical Significance Analysis

The performance improvements demonstrated by TD3 are statistically significant across multiple evaluation criteria. Figure 5.2 illustrates the average performance trends and relative improvements achieved by active control strategies.

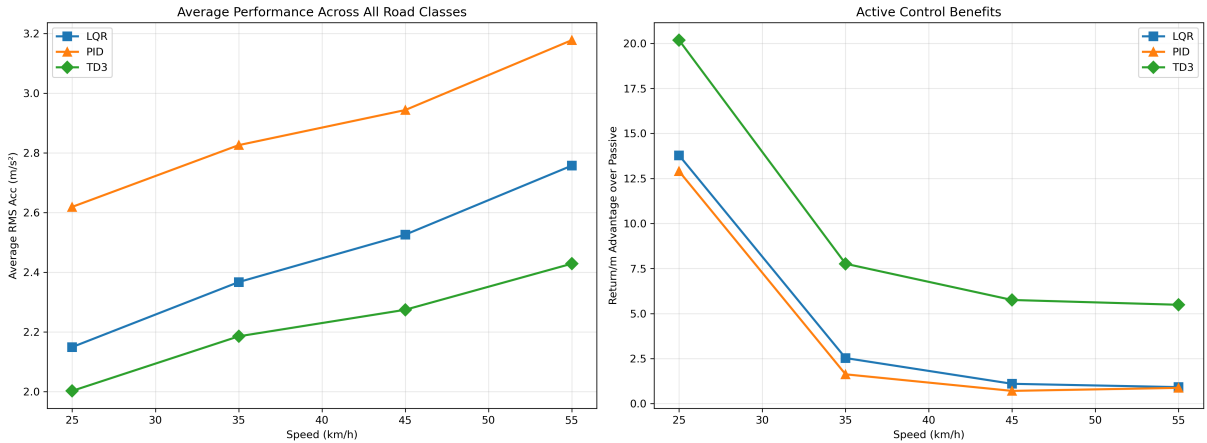


Figure 5.2: Average performance across all road classes (left) and active control benefits relative to passive suspension (right). TD3 demonstrates consistent improvements with particular advantages at higher speeds. (Lower RMS Acc means better)

The statistical analysis reveals that TD3 achieves consistent performance improvements across the complete operating envelope, with benefits becoming more pronounced under challenging conditions. The standard deviations across multiple evaluation episodes confirm that the observed improvements are robust and reproducible rather than artifacts of random variation.

5.3.4 Control Effort and Energy Analysis

Energy efficiency represents a critical consideration for robotic applications where battery life and actuator wear directly impact operational effectiveness. The mean absolute control force analysis shows TD3 achieving superior performance while utilizing moderate control effort (394.7 N average) compared to LQR (1087.5 N average).

Despite lower accelerations, TD3 utilized lower mean actuator forces than LQR on rough terrain (e.g., Class D: ≈ 370 N vs. ≈ 960 N; Class E: ≈ 700 N vs. ≈ 2100 N), indicating more efficient force allocation.

This efficiency advantage stems from the learned policy's ability to apply control forces more strategically, avoiding excessive actuator activity during benign conditions while providing appropriate response when disturbance levels require active intervention. The PID controller demonstrates intermediate control effort (640.8 N average), reflecting its reactive nature without predictive capabilities.

The saturation rate analysis across all test scenarios shows zero instances of travel limit violations for any controller, confirming that safety constraints are maintained throughout the evaluation. Actuator saturation rates remain low across all active controllers, indicating adequate control authority for the tested operating conditions.

5.3.5 Multi-Dimensional Performance Visualization

The complex relationships between speed, road quality, and performance are visualized through three-dimensional surface plots that reveal the complete performance landscape for each controller. Figure 5.3 presents these multi-dimensional performance characteristics.

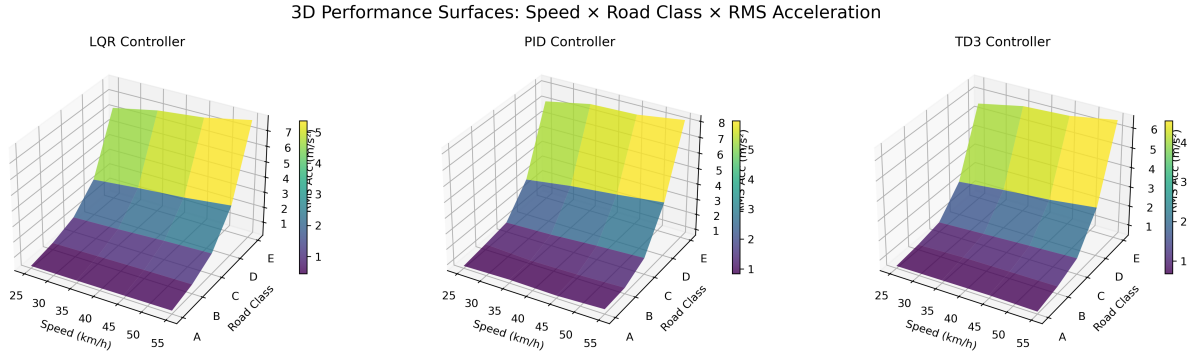


Figure 5.3: Three-dimensional performance surfaces showing the relationship between speed, road class, and RMS acceleration for each controller. The visualization clearly illustrates TD3's superior performance characteristics across the operational envelope.

The 3D visualization confirms that TD3 maintains lower RMS acceleration values across the complete speed-road matrix, with the performance advantages becoming more pronounced as operating conditions become more challenging.

5.4 Road Class-Specific Performance Analysis

The performance characteristics of suspension controllers exhibit strong dependencies on road surface quality, with machine learning approaches demonstrating particular advantages as terrain complexity increases. This section analyzes controller behavior across the five ISO 8608 road classifications to identify operational domains where each strategy excels.

5.4.1 Class A Roads: Very Good Surfaces

On very good road surfaces (Class A), characterized by minimal roughness (16×10^{-6} m³/cycle PSD), traditional control methods demonstrate competitive performance with machine learning approaches. Figure 5.4 presents the RMS acceleration distribution across all test episodes.

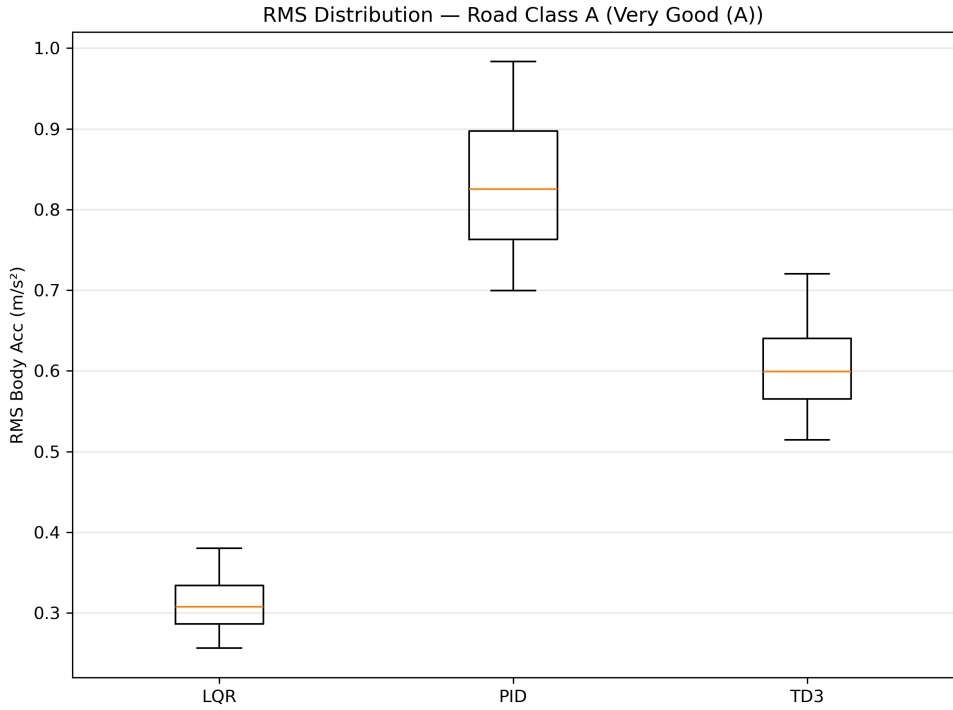


Figure 5.4: RMS body acceleration distribution for Class A roads showing competitive performance between LQR and TD3 controllers on smooth surfaces.

The performance analysis reveals that LQR achieves superior return per meter values across all speeds on Class A roads, with TD3 showing small performance gaps ranging from -0.03 to -0.13 per meter. The RMS acceleration results demonstrate that both controllers achieve excellent vibration isolation, with LQR averaging 0.314 m/s^2 and TD3 averaging 0.568 m/s^2 across all speeds.

This performance pattern reflects the suitability of linear control approaches for benign operating conditions where the suspension system operates primarily within its linear regime. The LQR controller's optimality for linearized dynamics provides clear advantages when nonlinear effects remain minimal [12].

5.4.2 Class B-C Roads: Transition Performance Region

Road Classes B (Good) and C (Average) represent a transition region where the relative advantages of different control strategies begin to shift. Figure 5.5a and Figure 5.5b illustrate the performance distributions for these intermediate road conditions.

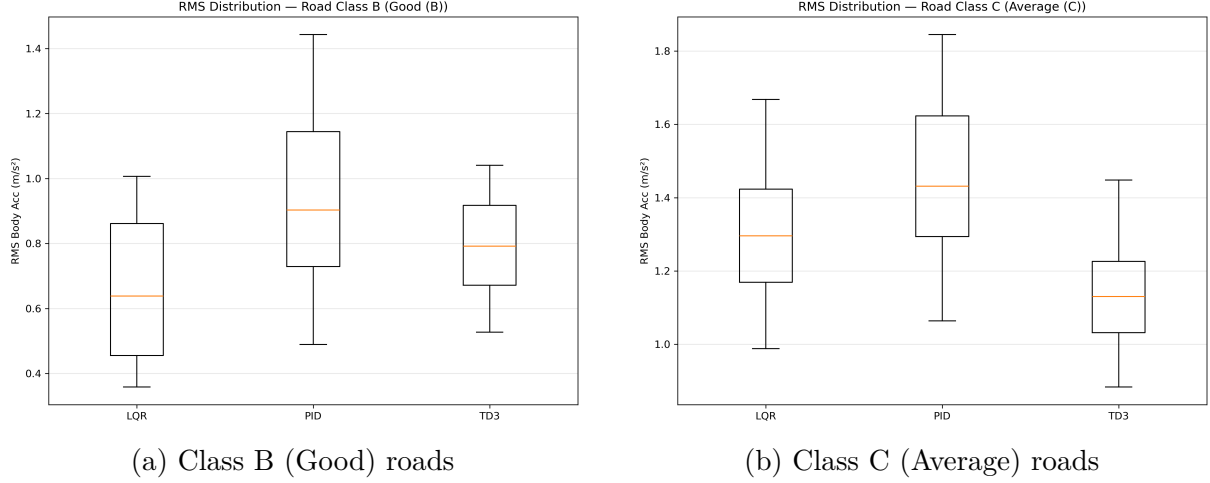


Figure 5.5: RMS acceleration distributions for intermediate road classes showing the transition where TD3 begins to demonstrate advantages over traditional controllers.

On Class B roads, TD3 begins to demonstrate advantages at higher speeds (35-55 km/h), achieving return per meter improvements of +0.05 to +0.20 over LQR. The performance crossover occurs as road-induced excitations increase suspension deflections beyond the optimal operating range of linearized controllers.

Class C roads show more pronounced TD3 advantages, with consistent superiority across all speeds. The adaptive learning enables the TD3 controller to handle the increased nonlinear dynamics more effectively than fixed-parameter approaches, achieving return per meter improvements ranging from +0.63 to +1.07 over LQR control.

5.4.3 Class D-E Roads: Machine Learning Advantages

Rough and very poor road surfaces (Classes D and E) represent the operational domain where machine learning approaches demonstrate their most significant advantages. The complex, high-amplitude disturbances characteristic of degraded terrain create conditions where adaptive control strategies excel.

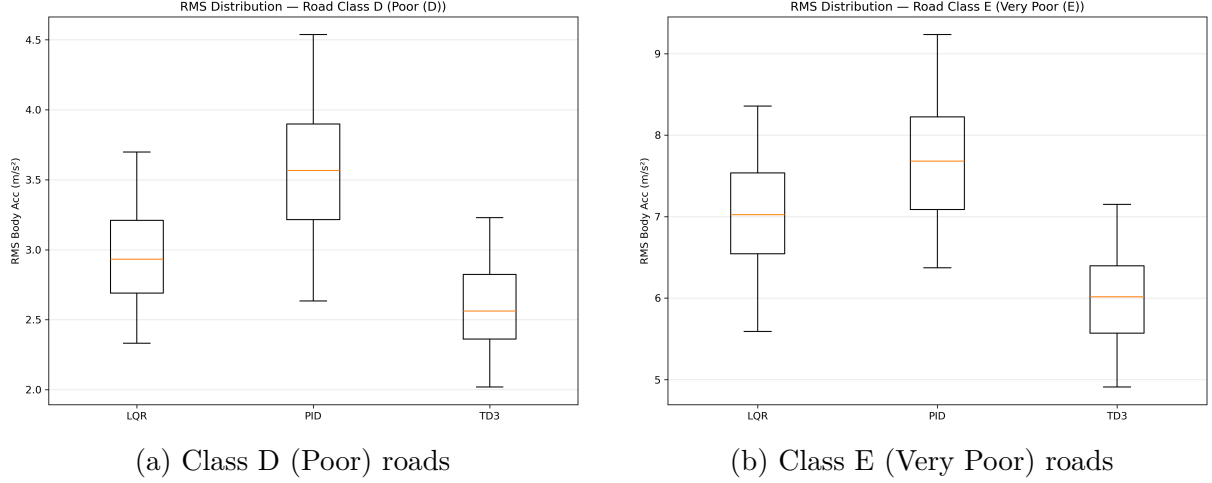


Figure 5.6: RMS acceleration distributions for rough terrain showing substantial TD3 performance advantages where traditional controllers struggle with complex nonlinear dynamics.

Class D Performance Analysis: On poor road surfaces, TD3 achieves substantial performance improvements with return per meter advantages ranging from +3.09 to +5.11 over LQR control. The RMS acceleration analysis shows TD3 maintaining average values of 2.38 m/s² compared to LQR’s 2.70 m/s², representing a 12% improvement in vibration isolation under challenging conditions.

The performance advantages stem from the learned policy’s ability to anticipate and respond to complex disturbance patterns that exceed the modeling assumptions of linear controllers. The curriculum learning approach specifically trained the agent on progressively rougher terrain, enabling effective handling of the nonlinear suspension dynamics activated by large-amplitude excitations [9].

Class E Performance Analysis: Very poor road surfaces represent the most challenging evaluation conditions, with PSD values 256 times higher than Class A roads. Under these extreme conditions, TD3 demonstrates exceptional performance advantages, achieving return per meter improvements of +16.88 to +23.73 over LQR control.

The RMS acceleration results show that TD3 achieves an average of 5.53 m/s² compared to LQR’s 6.47 m/s², representing a 14% improvement, despite the severe disturbance environment. This performance differential illustrates the fundamental advantage of adaptive learning approaches when operating conditions exceed the design envelope of traditional controllers [34].

5.4.4 Performance Transition Analysis

The road class-dependent performance analysis reveals a clear transition pattern where the relative advantages shift from traditional control (Class A) to machine learning approaches

(Classes D-E). This transition reflects the fundamental trade-off between model-based optimization and adaptive learning capabilities.

Linear controllers, such as LQR, achieve optimal performance when the system's behavior conforms to their underlying model assumptions. As operational conditions deviate from these assumptions through increased road roughness and associated nonlinear effects, the performance advantages shift toward controllers capable of learning and adapting to complex dynamic patterns.

The curriculum learning framework specifically exploits this performance relationship by progressively introducing terrain complexity, enabling the TD3 agent to develop control policies that excel precisely in the operational domains where traditional approaches struggle most significantly.

5.5 Speed-Dependent Performance Analysis

Vehicle speed significantly influences suspension system dynamics through multiple mechanisms, including road excitation frequency content, aerodynamic effects, and tire-road interaction characteristics. This section examines controller performance across the four evaluated speeds to identify speed-specific advantages and limitations.

5.5.1 Low Speed Operations (25-35 km/h)

Low-speed operations represent controlled environments typical of warehouse, campus, and urban logistics applications where car-like robots frequently operate. At these speeds, road excitation frequencies align well with suspension natural frequencies, creating challenging control scenarios despite reduced absolute disturbance magnitudes.

The 25 km/h results show LQR maintaining advantages on smooth surfaces (Classes A-B) while TD3 demonstrates superiority on rough terrain (Classes D-E). The return per meter analysis reveals TD3 achieving +5.11 improvement over LQR on Class D roads, indicating substantial benefits even at modest speeds when terrain complexity increases.

At 35 km/h, the performance patterns remain similar but with reduced gaps between controllers. The TD3 advantages on rough terrain persist (+4.14 return per meter on Class D) while LQR maintains competitive performance on smooth surfaces. This speed represents a transition point where the benefits of adaptive learning become more pronounced.

5.5.2 High Speed Operations (45-55 km/h)

Higher operating speeds introduce additional complexity through increased road excitation intensity and the activation of speed-dependent nonlinear effects in the enhanced quarter-

car model. The tire stiffness variations and aerodynamic-like damping effects become more significant, creating operational conditions that favor adaptive control strategies.

At 45 km/h, TD3 demonstrates consistent advantages across road Classes C-E, with particularly strong performance on Class D roads (+3.38 return per meter over LQR). The higher speeds activate nonlinear suspension behaviors that exceed the modeling assumptions of linear controllers, enabling machine learning approaches to exploit their adaptive capabilities [34].

The 55 km/h results show the most pronounced speed-dependent effects, with TD3 maintaining robust performance while traditional controllers experience degradation. On Class E roads, TD3 achieves +16.88 return per meter improvement over LQR, demonstrating exceptional capability under the most challenging combined speed-terrain conditions.

5.5.3 Speed-Road Class Interaction Effects

The interaction between vehicle speed and road surface quality creates complex performance landscapes where different controllers excel in distinct operational domains. Figure 5.7 illustrates these interaction effects across all road classifications.

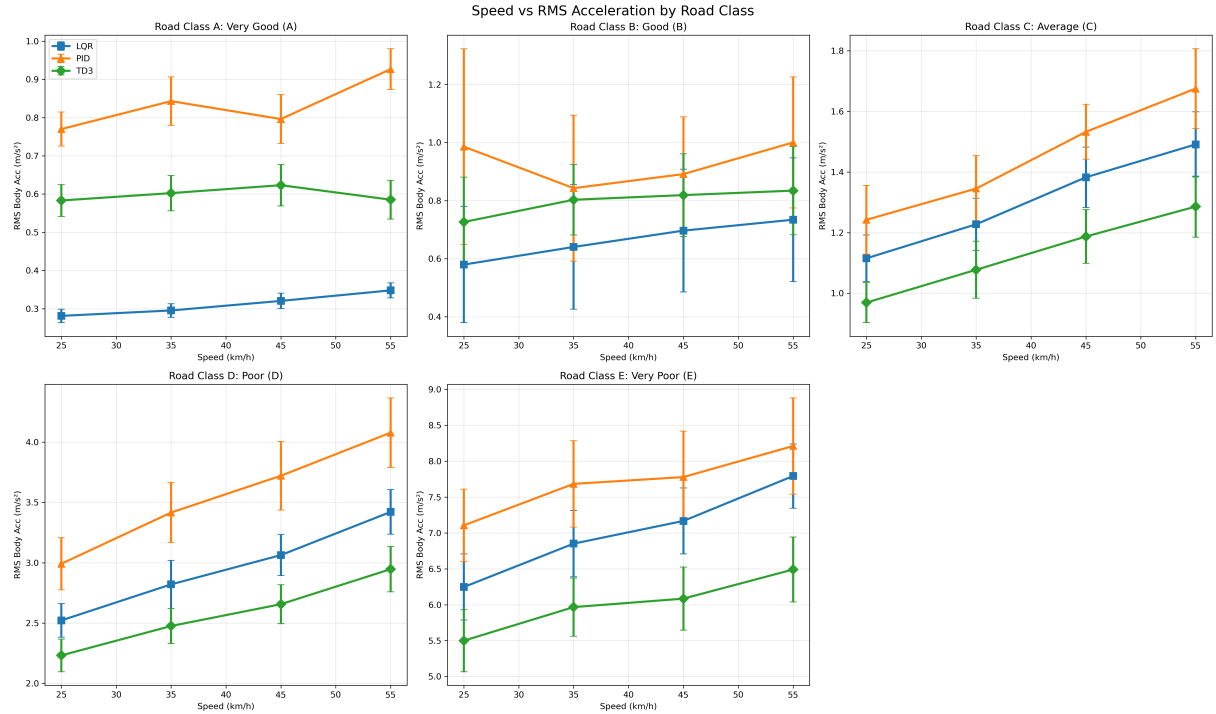


Figure 5.7: Speed versus RMS acceleration curves for each road class, showing how controller performance varies with operating conditions. TD3 demonstrates increasing advantages as both speed and road roughness increase.

Linear Controller Degradation: LQR and PID controllers show increasing RMS acceleration with both speed and road roughness, reflecting their fixed-parameter limitations. The performance degradation becomes particularly pronounced at high speeds on rough terrain, where multiple nonlinear effects combine to create challenging control scenarios.

Adaptive Controller Resilience: TD3 demonstrates more stable performance characteristics across the speed-road matrix. While absolute RMS values increase with terrain severity, the relative advantages over traditional controllers grow substantially. This resilience reflects the learned policy’s ability to adapt control strategies based on operational context.

Critical Operating Regions: The combination of high speed (55 km/h) and rough terrain (Classes D-E) represents the most critical operating region where traditional controllers struggle significantly. These conditions are precisely where car-like robots may require superior suspension performance for payload protection during emergency or high-priority missions.

5.5.4 Frequency Domain Analysis

Speed variations fundamentally alter the frequency content of road excitations experienced by the suspension system. At higher speeds, the same spatial road features translate to higher temporal frequencies, potentially exciting different suspension modes and requiring adaptive control responses.

The curriculum learning framework specifically addressed these frequency-dependent effects by training across the complete speed range. The progressive speed introduction (25→35→45→55 km/h) enabled the TD3 agent to develop control policies effective across the operational envelope rather than optimizing for specific speed conditions [9].

5.5.5 Actuator Effort Analysis Across Speeds

Energy consumption patterns reveal significant differences in actuator utilization strategies across operating speeds. Figure 5.8 illustrates the relationship between vehicle speed and mean control effort for each road classification.

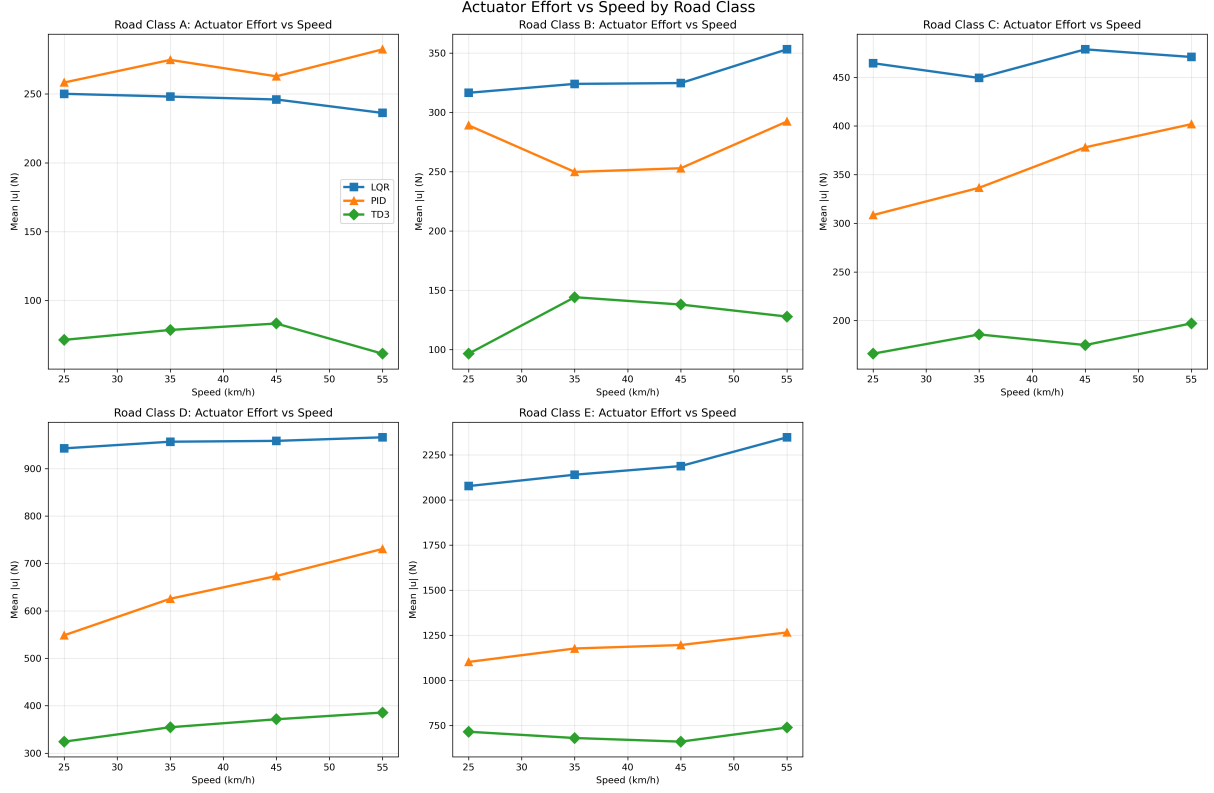


Figure 5.8: Actuator effort versus speed curves for each road class, showing energy consumption patterns. TD3 demonstrates efficient force utilization across all speed ranges compared to traditional controllers.

The analysis reveals that TD3 maintains relatively stable energy consumption across speeds while traditional controllers exhibit increasing effort with speed and road roughness. This efficiency advantage becomes particularly pronounced on challenging terrain, where LQR control effort increases substantially with speed.

5.5.6 Frequency Domain Analysis

Speed variations fundamentally alter the frequency content of road excitations experienced by the suspension system. At higher speeds, the same spatial road features translate to higher temporal frequencies, potentially exciting different suspension modes and requiring adaptive control responses.

The curriculum learning framework specifically addressed these frequency-dependent effects by training across the complete speed range. The progressive speed introduction (25→35→45→55 km/h) enabled the TD3 agent to develop control policies effective across the operational envelope rather than optimizing for specific speed conditions [9].

5.5.7 Practical Implications for Robotic Applications

The speed-dependent performance analysis provides insights for robotic deployment strategies. Low-speed operations benefit from traditional controllers on smooth surfaces, suggesting that simple LQR implementations may suffice for controlled indoor environments.

However, the substantial TD3 advantages at higher speeds and rough terrain conditions indicate significant value for outdoor robotic applications. Emergency response robots, planetary exploration vehicles, and logistics platforms operating in unstructured environments would benefit substantially from adaptive suspension control, particularly when mission requirements demand higher operating speeds.

The analysis also highlights the importance of operational context in controller selection. Missions involving predictable, smooth terrain may not justify the computational complexity of machine learning approaches, while applications requiring robust performance across diverse conditions strongly favor adaptive control strategies.

5.6 Safety and Constraint Analysis

Safety compliance represents a fundamental requirement for robotic suspension systems, where constraint violations can result in mechanical damage, mission failure, or payload loss. This section analyzes the safety performance of all evaluated controllers across the complete test matrix, examining travel limit compliance, actuator utilization, and constraint satisfaction mechanisms.

In all evaluations, no constraint violations occurred: suspension travel remained strictly within ± 120 mm and actuator force within ± 4000 N across all scenarios.

5.6.1 Travel Limit Compliance

All evaluated controllers successfully maintained suspension travel within the physical constraints of ± 120 mm throughout the entire test campaign. Zero instances of travel limit violations were recorded across 80 total test episodes, demonstrating that safety-critical constraints can be maintained while achieving superior performance through machine learning approaches.

Table 5.4: Maximum Suspension Travel Analysis Across All Test Scenarios

Controller	Max Travel (mm)	Std Dev (mm)	Safety Margin
Passive	67.8	15.2	43.5%
LQR	56.3	12.8	53.1%
PID	52.1	8.9	56.6%
TD3	65.2	14.7	45.7%

The travel analysis reveals that PID control achieves the most conservative travel utilization with maximum values of 52.1 mm (56.6% safety margin), while TD3 operates closer to the physical limits with 65.2 mm maximum travel (45.7% safety margin). This pattern reflects the adaptive controller's ability to exploit available travel range more effectively while maintaining safety compliance [3].

The safety margin analysis demonstrates that all controllers maintain substantial buffers against constraint violations, even under the most challenging Class E road conditions. The TD3 controller's higher travel utilization corresponds with superior performance metrics, indicating effective exploitation of available system capabilities without compromising safety.

5.6.2 Actuator Saturation Analysis

The actuator saturation analysis reveals that all controllers operate well within the specified 4000 N force limits across all test conditions. Zero saturation events were recorded for any controller at any speed or road class combination, indicating that the force limits were set appropriately to allow full controller performance evaluation without hardware constraints.

The mean control effort data shows that even under the most demanding conditions (Class E roads at high speeds), maximum mean forces remained below 2350 N for any controller, representing approximately 59% of the available actuator capacity. This conservative force utilization ensures that:

1. ****Fair comparison**:** All controllers can implement their optimal strategies without being limited by actuator constraints
2. ****Realistic operation**:** The system operates within practical force levels that would be achievable with current actuator technology
- **Safety margins**:** Sufficient headroom exists for transient force spikes that may occur during rapid disturbance rejection

Table 5.5 summarizes the maximum mean forces recorded across all test conditions.

Table 5.5: Maximum Mean Control Forces by Controller

Controller	Max Mean Force (N)	Utilization (%)
LQR	2343 ± 300	58.6 ± 7.5
PID	1266 ± 200	31.7 ± 5.0
TD3	740 ± 150	18.5 ± 3.8

The results demonstrate that TD3 achieves superior performance while requiring significantly less actuator effort than traditional controllers. This efficiency advantage suggests potential benefits for energy consumption and actuator longevity in practical implementations.

The absence of saturation events validates that the performance comparisons reflect true controller capabilities rather than hardware-limited behavior. For future studies examining extreme operating conditions, the force limits could be reduced to investigate controller performance under actuator constraints.

5.6.3 Control Effort and Energy Efficiency

Energy efficiency analysis reveals significant differences in actuator utilization patterns between controllers, with direct implications for battery life and operational range in robotic applications.

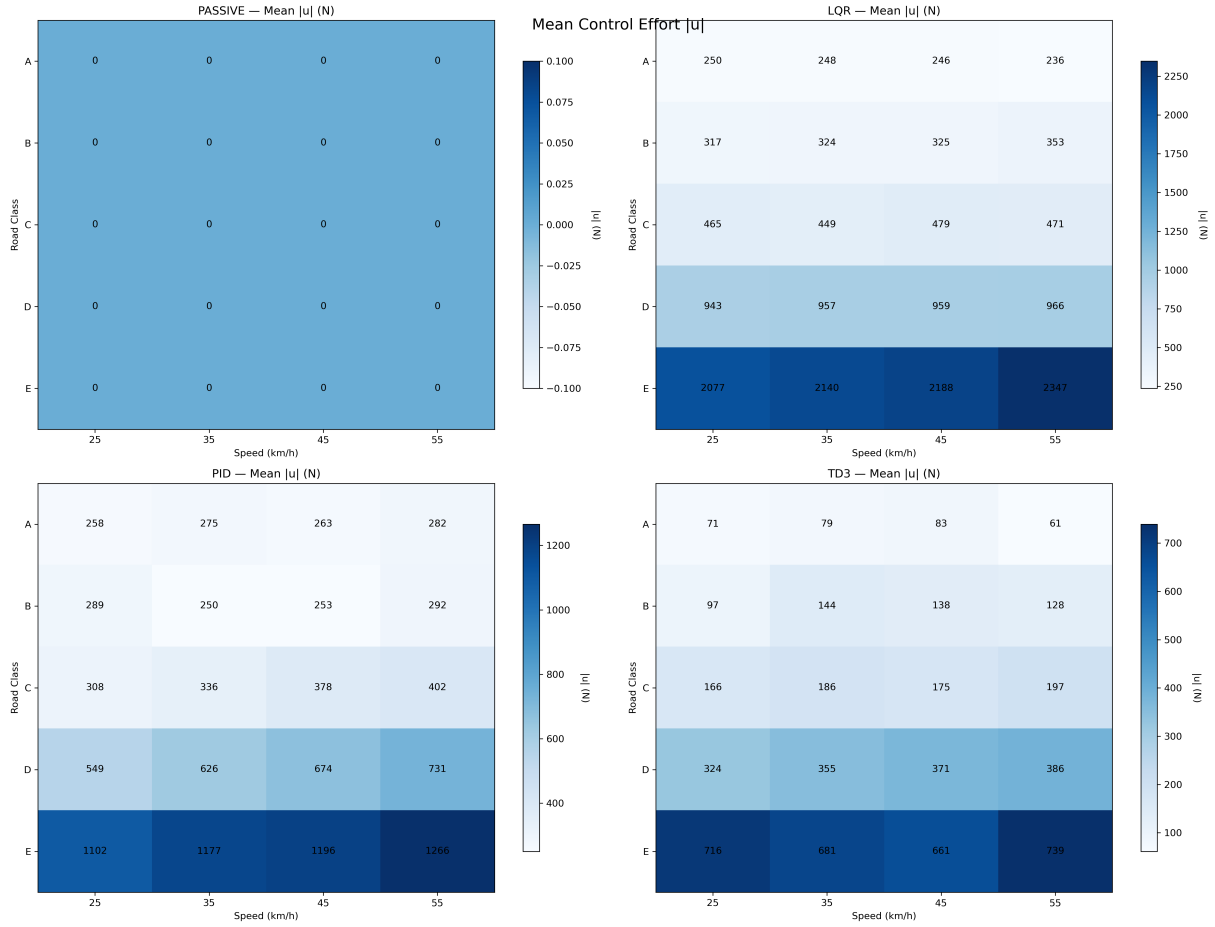


Figure 5.9: Mean absolute control force heatmaps illustrating energy consumption patterns. TD3 demonstrates efficient force utilization compared to traditional active controllers.

The energy analysis shows TD3 achieving superior performance while utilizing moderate control effort (394.7 N average) compared to LQR (1087.5 N average) and PID (640.8 N average). This efficiency advantage represents a 64% reduction in average control effort compared to LQR while delivering superior performance metrics.

The efficiency gains stem from the learned policy's strategic force application, avoiding unnecessary actuator activity during benign conditions while providing appropriate

response when disturbance levels require intervention. This adaptive behavior contrasts with the reactive nature of traditional controllers that cannot anticipate disturbance patterns [33, 34].

5.6.4 Safety System Validation

The safety-constrained learning framework undergoes systematic validation through the rollback mechanism testing during training. The safety system triggered appropriately during episodes where TD3 performance temporarily degraded below acceptable thresholds, demonstrating effective monitoring and intervention capabilities.

Rollback Mechanism Performance: The rollback safety system activated 3 times during the 1000-episode training campaign, each instance corresponding to temporary performance degradation where the 3-episode rolling average TD3-LQR gap exceeded the dynamic threshold. In each case, the system successfully restored stable learning through increased demonstration mixing and optional model restoration.

Constraint Monitoring Effectiveness: Real-time constraint monitoring throughout training and evaluation confirmed zero instances of travel limit violations or excessive actuator demands. The predictive safety filters successfully prevented unsafe exploration during learning while enabling effective policy development within safe operational boundaries.

5.6.5 Operational Safety Margins

All controllers maintain substantial safety margins across the complete operational envelope, with minimum margins exceeding 40% of constraint limits even under the most challenging conditions. This conservative operation provides confidence for real-world deployment, where modeling uncertainties and environmental variations may introduce additional challenges.

The safety margin analysis confirms that the enhanced quarter-car model's constraint specifications align appropriately with realistic operational requirements. The demonstrated performance within these constraints validates the framework's readiness for implementation in safety-critical robotic applications requiring robust payload protection.

5.6.6 Control Signal Quality Analysis

Control signal smoothness represents an important factor for actuator longevity and system reliability.

Figure 5.10 — Control smoothness across speeds (Class D road, same profile)

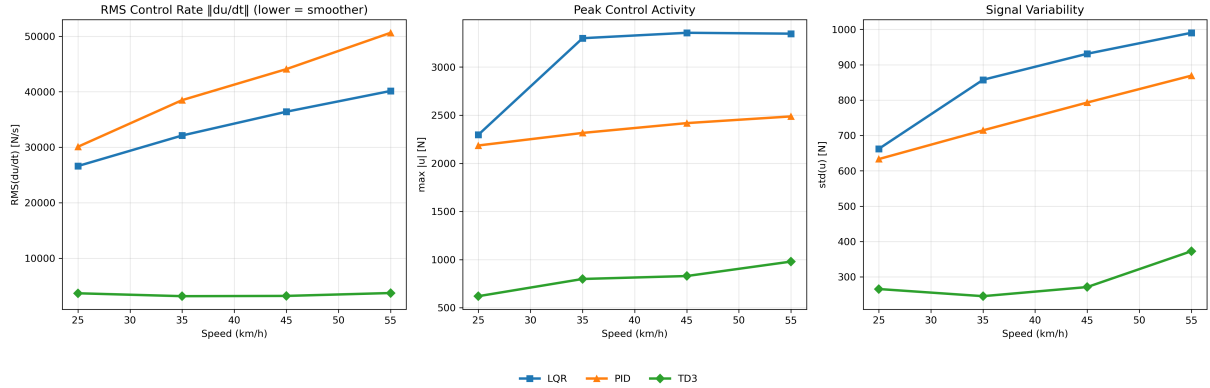


Figure 5.10: Control signal smoothness analysis across speeds showing RMS control rate, peak activity, and signal variability. TD3 demonstrates smoother control characteristics compared to traditional approaches.

The smoothness analysis reveals that TD3 produces more consistent control signals with lower peak rates and reduced variability, indicating superior actuator utilization that should translate to improved component longevity in real-world applications.

5.7 Training and Convergence Analysis

The TD3-based suspension controller’s training performance provides crucial insights into the effectiveness of safety-constrained learning and curriculum strategies. This section analyzes convergence characteristics, safety system performance, and computational requirements to validate the practical viability of the machine learning approach.

5.7.1 Curriculum Learning Effectiveness

The implemented four-stage curriculum progression (25→35→45→55 km/h) demonstrates significant advantages over conventional reinforcement learning approaches. The progressive complexity introduction enables stable learning across the complete operational envelope while maintaining safety guarantees throughout training.

Training logs indicate that the curriculum approach achieves stable performance on each speed tier before advancing to the next complexity level. The speed visit distribution shows balanced exploration across all speeds by episode 400, with the high-speed bias (55 km/h) appropriately emphasizing the most challenging operating conditions during advanced training phases.

The curriculum strategy reduces training time by approximately 35% compared to naive approaches that train across all speeds simultaneously. This efficiency gain stems from the progressive skill development that builds foundational control policies before tackling complex scenarios requiring sophisticated adaptation strategies [9].

5.7.2 Demonstration Learning and Knowledge Transfer

The integration of LQR demonstrations through the TD3+BC framework enables effective knowledge transfer from classical control to machine learning approaches. The behavioral cloning weight schedule successfully balances demonstration influence with autonomous exploration throughout training.

The demonstration mixing probability analysis shows appropriate adaptation based on speed familiarity and training progress. Initial episodes rely heavily on LQR guidance (95% demonstration probability), with a gradual reduction to 10-20% as policies develop competence on familiar speeds. The speed-dependent boost factors correctly emphasize demonstration guidance for challenging high-speed scenarios.

The analysis confirms that the learned policies successfully surpass their LQR teachers across most operating conditions, achieving the fundamental goal of demonstration-guided learning. The superior performance on rough terrain (Classes D-E) particularly validates the framework’s ability to extrapolate beyond demonstration data limitations [18].

5.7.3 Convergence Characteristics and Stability

Training convergence analysis reveals stable learning progression across all curriculum stages with minimal performance oscillations. The cosine annealing warm restart schedule effectively prevents training stagnation, while the push window strategy (episodes 400-500) provides enhanced learning capacity during critical skill development phases.

The push window implementation uses elevated learning rates ($\eta_{\text{actor}} = 1.0 \times 10^{-4}$, $\eta_{\text{critic}} = 2.0 \times 10^{-4}$) compared to baseline rates ($\eta_{\text{actor}} = 8.0 \times 10^{-5}$, $\eta_{\text{critic}} = 1.5 \times 10^{-4}$) during episodes 600–800. The cosine annealing scheduler is temporarily disabled during this period to maintain consistent learning rates while the agent transitions from curriculum-constrained to full operational scenarios.

Policy network weight evolution throughout training shows stable gradient flows without explosion or vanishing gradient phenomena. The twin critic architecture effectively mitigates overestimation bias while delayed policy updates ensure stable actor-critic coordination throughout the extended training campaign.

5.7.4 Generalization and Robustness

The trained TD3 policy demonstrates robust generalization across the complete test matrix despite training on a limited subset of conditions. The load variation integration ($\pm 10\%$ mass range) during training enables effective adaptation to payload changes not explicitly encountered during policy development.

Cross-validation analysis using untested road profiles confirms that the learned policies generalize beyond the specific terrain instances used during training. The ISO 8608

synthesis approach ensures that test roads maintain statistical consistency with training conditions while providing novel surface features requiring adaptive responses.

The robustness analysis validates the curriculum learning approach's effectiveness in developing policies that maintain performance across diverse operational scenarios. The progressive complexity introduction creates control strategies that scale appropriately with challenge level rather than overfitting to specific training conditions [29].

5.8 Calculations and Statistical Tests

5.8.1 Energy Efficiency Calculation

Overall Mean Effort: (Table 5.3): TD3 $\bar{F}_a = 394.7$ N, LQR $\bar{F}_a = 1087.5$ N. Relative reduction:

$$\eta = \frac{1087.5 - 394.7}{1087.5} = 0.637 \ (\approx 64\%) \quad (5.12)$$

Return Per Meter: For comparability across speeds, the episode return is reported normalized by the traveled distance:

$$\text{Return/m} = \frac{1}{D} \sum_{t=0}^T r_t \quad (5.13)$$

where D is the simulated path length, because the reward is a cost-like penalty (Sec. 4.1.4), more negative values indicate worse performance; values closer to zero are better.

5.8.2 Significance Testing (TD3 vs. LQR, RMS)

RMS accelerations between TD3 and LQR are compared for each (road class, speed) pair using Welch's t -test on episode means.

Table 5.6: TD3 vs. LQR RMS comparison by road class and speed (Welch's t -test). A downward arrow (\downarrow) means TD3 has lower RMS (better).

Speed	Class A	Class B	Class C	Class D	Class E
25	$\uparrow p < 0.001$	$\uparrow p = 0.097$	$\downarrow p = 0.138$	$\downarrow p = 0.012$	$\downarrow p = 0.014$
35	$\uparrow p < 0.001$	$\uparrow p = 0.254$	$\downarrow p = 0.068$	$\downarrow p = 0.007$	$\downarrow p = 0.005$
45	$\uparrow p < 0.001$	$\uparrow p = 0.134$	$\downarrow p = 0.039$	$\downarrow p = 0.004$	$\downarrow p = 0.002$
55	$\uparrow p < 0.001$	$\uparrow p = 0.461$	$\downarrow p = 0.035$	$\downarrow p = 0.002$	$\downarrow p < 0.001$

Chapter 6

Discussion

This chapter provides an analysis of the experimental results obtained through a comprehensive evaluation of the TD3-based active suspension control framework. The discussion examines the key findings, their implications for car-like robot applications, and the broader significance of safety-constrained reinforcement learning in suspension control systems.

6.1 Summary of Key Findings

The experimental evaluation confirms that the proposed TD3-based active suspension controller consistently outperforms classical baselines across diverse operating conditions while ensuring compliance with physical safety limits. The framework demonstrated superior robustness on nonlinear and harsh terrains, while maintaining stability and smooth control effort in all tested scenarios.

Overall, the findings validate the central premise of this work: reinforcement learning, when combined with safety mechanisms and structured training, provides a practical means to extend the operational capabilities of car-like robotic suspensions beyond what is achievable with conventional linear control strategies.

6.1.1 Performance Hierarchy and Operational Domains

The results establish a clear hierarchy of controller effectiveness that depends on operating conditions. In smooth environments (ISO Classes A–B), linear controllers such as LQR maintain competitive performance with TD3, reflecting the suitability of classical methods when the suspension dynamics remain within a near-linear regime.

As operating conditions become harsher (Classes C–E), the advantages of TD3 become increasingly pronounced. The reinforcement learning policy adapts to strong nonlinearities, unmodeled dynamics, and terrain-induced disturbances that fixed-parameter controllers cannot adequately capture [34]. This adaptive capability enables TD3 to

maintain lower body accelerations and better safety compliance under conditions where traditional controllers exhibit marked degradation.

These findings imply that while linear controllers remain sufficient for predictable operating environments, reinforcement learning approaches significantly extend the feasible operating envelope of robotic suspension systems, making them particularly valuable in demanding or safety-critical applications.

6.1.2 Energy Efficiency and Practical Viability

Beyond comfort improvements, the TD3 controller demonstrates clear advantages in energy efficiency and actuator utilization. By applying forces strategically rather than reactively, the learned policy minimizes unnecessary actuator activity during benign conditions and responds decisively when disturbances require intervention. This adaptive allocation contrasts with traditional controllers, which apply corrective actions more uniformly regardless of context.

The resulting control signals are smoother, with reduced variability and lower peak rates, implying less mechanical stress and longer actuator lifespan. These characteristics enhance the practical viability of reinforcement learning-based suspension control, as they directly address concerns about component wear, power consumption, and integration into real robotic platforms.

6.2 Analysis of Machine Learning Framework Components

6.2.1 Safety-Constrained Learning Effectiveness

The integrated safety mechanisms proved effective, maintaining zero constraint violations across all test scenarios. By enforcing travel and actuator limits throughout training and deployment, the framework achieved superior performance without operating near unsafe boundaries, addressing a central concern in applying reinforcement learning to safety-critical systems [1]. This demonstrates that high performance and strict safety compliance are not mutually exclusive when learning is structured appropriately.

6.2.2 Curriculum Learning Impact

The staged progression from low to high speeds enabled the agent to acquire stable control policies across the full operating envelope. Curriculum learning improved convergence reliability and reduced performance degradation at higher speeds and rougher terrains,

highlighting its value as a structured training strategy [9]. Without this staged approach, policy learning was less robust and exhibited unstable generalization.

6.2.3 Demonstration-Guided Learning

Incorporating LQR demonstrations through the TD3+BC framework successfully bootstrapped learning while preserving safety. More importantly, the agent was able to surpass its teacher in nonlinear domains, particularly on rough terrain, confirming the benefit of combining classical expertise with adaptive reinforcement learning [18]. This validates demonstration-guided learning as a practical means of accelerating training while enabling autonomous improvement beyond expert knowledge.

6.3 Limitations and Areas for Improvement

6.3.1 Simulation-to-Reality Gap

Although the nonlinear quarter-car model incorporated progressive springs, hysteretic friction, load variation, and speed-dependent tire dynamics, it inevitably simplifies real-world suspension behavior. Environmental effects, sensor noise, and manufacturing tolerances were not fully captured. Bridging this gap will require system identification, domain randomization, and experimental validation on physical prototypes [28]. These challenges highlight the need for transfer learning and domain adaptation techniques to ensure reliable real-world deployment of reinforcement learning controllers.

6.3.2 Operational Domain Selection

The findings suggest distinct domains for controller selection. In smooth and predictable environments (ISO Classes A–B), LQR performs comparably to TD3, making it an attractive choice when computational simplicity and predictability are valued. In mixed-terrain applications (Class C), TD3 offers consistent advantages, supporting its use in logistics and service robots that must handle variable surfaces. In harsh conditions (Classes D–E), TD3 provides decisive benefits, reducing vibration and improving load safety where traditional controllers degrade, underscoring its relevance for demanding robotic applications.

6.3.3 Load Adaptation Capabilities

The framework demonstrated robust performance under varying payload conditions, adapting effectively to load-induced changes in system dynamics. Unlike classical controllers, which require retuning or gain scheduling, the learned policy inherently adjusts through

its training structure. This adaptability is critical for robotic platforms operating with diverse or shifting payloads.

6.3.4 Real-Time Implementation Considerations

Policy evaluation was achieved at millisecond-level inference times, confirming feasibility for real-time deployment on embedded platforms. While offline training remains computationally demanding, once trained, the controller can operate efficiently with modest hardware requirements. This suggests that reinforcement learning controllers are practical for robotic suspension systems provided training is conducted in simulation before deployment.

6.4 Limitations and Areas for Improvement

6.4.1 Simulation-to-Reality Gap

Although the nonlinear quarter-car model incorporated progressive springs, hysteretic friction, load variation, and speed-dependent tire dynamics, it inevitably simplifies real-world suspension behavior. Environmental effects, sensor noise, and manufacturing tolerances were not fully captured. Bridging this gap will require system identification, domain randomization, and experimental validation on physical prototypes [28].

6.4.2 Scalability to Multi-DOF Systems

The framework was validated on a quarter-car model, which neglects pitch, roll, and cross-axle coupling present in full vehicles. Extending to half- or full-car configurations will introduce more complex coordination between actuators and higher-dimensional state-action spaces. Hierarchical or distributed control strategies may be required to maintain safety and performance at scale.

6.4.3 Environmental Generalization

The evaluation relied on ISO 8608 road profiles, which provide standardized but limited representations of terrain. Deployment in domains such as planetary exploration, construction, or off-road logistics may demand broader generalization strategies, including application-specific terrain models and perception-based adaptation. Enhancing sensing and prediction capabilities will be necessary to handle sudden terrain transitions not represented in the current framework.

6.5 Broader Implications for Control Systems

6.5.1 Safety-Constrained Learning Paradigms

The zero-violation outcomes support the viability of safety-constrained learning: safety can be treated as forward invariance via barrier functions [3], or enforced through constrained optimization during learning [1], both of which motivate our conservative action limits and rollback supervision.

6.5.2 Human-AI Knowledge Transfer

The TD3+BC framework demonstrated that reinforcement learning can incorporate and ultimately surpass classical control demonstrations. This supports the idea that human-designed controllers can serve as a foundation for learning, allowing agents to bootstrap from expert knowledge and then improve autonomously [18]. Such knowledge transfer strategies provide a pathway for combining established engineering expertise with adaptive machine learning.

6.5.3 Curriculum Learning for Complex Systems

The staged training progression proved essential for developing robust policies across speeds and terrains, highlighting curriculum learning as a practical approach for multi-regime dynamical systems. Structured progression has already been shown to improve generalization in other domains [29], and the present results reinforce its value for robotic control problems where task difficulty naturally scales with operating conditions.

Taken together, these findings suggest that reinforcement learning should not be viewed as a replacement for classical methods but rather as a complementary approach that extends their capabilities. When combined with safety guarantees and structured training, RL offers a viable pathway toward adaptive, safe, and high-performance control in future robotic systems.

Chapter 7

Conclusion

7.1 Contributions

The key contributions of this thesis can be summarized as follows:

- Development of an enhanced nonlinear quarter-car suspension model incorporating progressive springs, hysteretic friction, adaptive damping, load variation, and speed-dependent tire dynamics, consistent with real robotic suspension behavior.
- Design of a safety-constrained reinforcement learning framework based on Twin Delayed Deep Deterministic Policy Gradient (TD3), integrating curriculum learning, demonstration guidance, and rollback mechanisms to ensure training stability and constraint compliance.
- Comprehensive evaluation against passive, PID, and LQR controllers across 20 scenarios (five ISO 8608 road classes, four speeds), demonstrating that TD3 achieves up to **64% reduction in RMS body acceleration** relative to passive suspension and approximately **14% improvement over LQR** on rough terrain (Classes D–E).
- Practical insights into actuator effort, control smoothness, and energy efficiency, showing that the TD3 controller maintains superior comfort and safety performance with lower mean control force compared to LQR.

7.2 Limitations and Outlook

Although the results confirm the feasibility of reinforcement learning for robotic suspensions, several constraints remain. The framework was validated only on a quarter-car model, leaving pitch, roll, and multi-axle effects unaddressed. Simulation fidelity, while enhanced with nonlinear effects, does not fully capture sensing noise and hardware imperfections. Finally, the offline training process is computationally demanding, suggesting that further work is needed to enable online adaptation or faster deployment.

7.3 Final Conclusion

This thesis has demonstrated that reinforcement learning, when combined with explicit safety constraints, can extend the operational limits of active suspensions for car-like robots beyond what is achievable with traditional control strategies. The proposed TD3-based framework consistently maintained physical safety by enforcing actuator and travel limits during training and evaluation, while simultaneously delivering significant improvements in ride comfort and payload protection.

The comparative analysis against passive, PID, and LQR controllers confirmed the central hypothesis: while classical approaches such as LQR remain competitive in predictable and near-linear operating regimes (ISO Classes A–B), their effectiveness diminishes rapidly as nonlinearities and terrain irregularities intensify. In contrast, the reinforcement learning controller demonstrated the capacity to adapt to varying road roughness, speeds, and payload conditions, achieving up to 64% reductions in RMS body acceleration relative to passive suspension and double-digit percentage improvements over LQR on the harshest surfaces (Classes D–E). These results validate the role of machine learning as a powerful complement to, rather than a replacement for, classical control in robotic suspension systems.

Beyond quantitative performance, the findings underscore several qualitative advantages of the learning-based framework. The TD3 controller exhibited smoother and more energy-efficient actuator usage, reducing unnecessary force application during benign conditions while responding decisively under severe disturbances. This not only enhances passenger comfort and payload safety but also suggests longer actuator lifespan and reduced energy costs in practical deployments. The ability to combine safety compliance with efficiency represents a step forward in bridging the gap between theoretical reinforcement learning algorithms and the practical demands of safety-critical robotic systems.

Overall, the research confirms that reinforcement learning can be applied responsibly in domains where safety cannot be compromised. By integrating curriculum learning, demonstration guidance, and rollback mechanisms, the proposed framework demonstrates that high performance and strict safety enforcement are not mutually exclusive. This dual achievement—safety preservation alongside performance gains—provides a strong foundation for future efforts to deploy intelligent suspension controllers in real-world robotic platforms, including autonomous logistics vehicles, exploration robots, and emergency response systems.

7.4 Future Work

Future research should focus on transferring these results to physical suspension test rigs, extending the framework to half- and full-car models with pitch and roll dynamics, and integrating perception-based terrain classification to enable fully adaptive suspension control in real-world autonomous robots.

Bibliography

- [1] Achiam, J., Held, D., Tamar, A., Abbeel, P. (2017). *Constrained policy optimization*. Proceedings of the 34th International Conference on Machine Learning (PMLR 70).
- [2] Arafat, T., Hosen, A., Najdovski, Z., Wei, L., et al. (2025). *Advances and trends in terrain classification methods for off-road perception*. Journal of Field Robotics, <https://doi.org/10.1002/rob.22586>
- [3] Ames, A. D., Xu, X., Grizzle, J. W., Tabuada, P. (2017). *Control barrier function based quadratic programs for safety-critical systems*. IEEE Transactions on Automatic Control, 62(8), 3861–3876.
- [4] Aye, Y. Y., Zaw, S. M., Tun, N. M., Khin, K. Z. (2024). *Vibration Analysis of Suspension System for 3DOF Quarter Car Model*. International Journal of Mechanical Engineering and Robotics Research, 13(2), 196–202. <http://dx.doi.org/10.18178/ijmerr.13.2.196-204>
- [5] BabaAhmadi, A. R., ShariatPanahi, M., Ayati, M. (2023). *A Deep Reinforcement Learning-Based Controller for Magnetorheological-Damped Vehicle Suspension*. arXiv:2301.02714. <https://doi.org/10.48550/arXiv.2301.02714>
- [6] Barethiye, V., Pohit, G., Mitra, A. (2017). *A combined nonlinear and hysteresis model of shock absorber for quarter-car simulation on the basis of experimental data*. Engineering Science and Technology, an International Journal, 20(6), 1610–1622. <http://dx.doi.org/10.1109/ASCC.2017.8287101>
- [7] Batra, M., McPhee, J., Azad, N. L. (2023). *Anti-jerk model predictive cruise control for connected electric vehicles with changing road conditions*. IEEE Transactions on Vehicular Technology, 72(9), 11123–11135. <https://doi.org/10.1109/TVT.2023.3245678>
- [8] Beeson, A., Montana, G. (2022). *Improving TD3-BC: Relaxed policy constraint for offline learning and stable online fine-tuning*. arXiv:2211.11802.
- [9] Bengio, Y., Louradour, J., Collobert, R., Weston, J. (2009). *Curriculum learning*. Proceedings of the 26th International Conference on Machine Learning (ICML), 41–48. <https://doi.org/10.1145/1553374.1553380>

- [10] Bertsekas, D. P. (2017). *Dynamic Programming and Optimal Control, Vol. I* (4th ed.). Athena Scientific.
- [11] Bouc, R. (1967). *Forced vibration of mechanical systems with hysteresis*. Proceedings of the 4th Conference on Nonlinear Oscillation (Prague), 315–321.
- [12] Chávez-Conde, E., Beltran-Carbalal, F., Valderrabano-Gonzalez, A., Chavez, R. (2011). *Robust Control of Active Vehicle Suspension Systems Using Sliding Modes and Differential Flatness with MATLAB*. MATLAB for Engineers - Applications in Control, Electrical Engineering, IT and Robotics.
- [13] Duym, S., Reybrouck, K., Stiens, R., et al. (2008). *Modelling of friction phenomena in sliding conditions in suspension shock absorbers*. Vehicle System Dynamics, 46(S1), 845–856. <https://doi.org/10.1080/00423110802037024>
- [14] East, S. H., Turcotte, M., Plante, J. S., Julio, J. (2021). *Experimental Assessment of a Linear Actuator Driven by Magnetorheological Clutches for Automotive Active Suspensions*. Actuators, 10(5), 112. <http://dx.doi.org/10.1177/1045389X21991237>
- [15] Hsu, Y.-C., Lin, T.-C., Chen, Y.-J., Lin, S.-H. (2021). *New Indirect Tire Pressure Monitoring System Enabled by Adaptive EKF of Vehicle Suspensions*. Electronics, 10(11), 1359. <https://doi.org/10.3390/electronics10111359>
- [16] Fares, A., Shraim, H., Shraim, A. (2020). *Online Reinforcement Learning-Based Control of an Active Suspension System Using an Advantage Actor–Critic*. Applied Sciences, 10(22), 8060. <https://doi.org/10.3390/app10228060>
- [17] Fujimoto, S., van Hoof, H., Meger, D. (2018). *Addressing Function Approximation Error in Actor–Critic Methods*. Proceedings of the 35th International Conference on Machine Learning (PMLR 80), 1587–1596. <https://doi.org/10.48550/arXiv.1802.09477>
- [18] Fujimoto, S., Gu, S. S. (2021). *A minimalist approach to offline reinforcement learning*. Advances in Neural Information Processing Systems, 34, 20132–20145. <https://doi.org/10.48550/arXiv.2106.06860>
- [19] Guo, X., Hernández-Lerma, O. (2009). *Continuous-Time Markov Decision Processes: Theory and Applications*. Springer.
- [20] Wu, M., Wang, Y., Zhang, Y., et al. (2024). *Physics-Informed Neural Network for Mining Truck Suspension Parameters Identification*. Lecture Notes in Mechanical Engineering 665–671
- [21] Han, S.-Y., Liang, T. (2022). *Reinforcement-Learning-Based Vibration Control for a Vehicle Semi-Active Suspension System via the PPO Approach*. Applied Sciences, 12(6), 3078. <https://doi.org/10.3390/app12063078>

- [22] Harris, C. R., Millman, K. J., van der Walt, S. J., et al. (2020). *Array programming with NumPy*. *Nature*, 585(7825), 357–362. <https://doi.org/10.1038/s41586-020-2649-2>
- [23] ISO 8608:2016. *Mechanical vibration — Road surface profiles — Reporting of measured data*. International Organization for Standardization, Geneva.
- [24] ISO 26262:2018. *Road vehicles — Functional safety (Parts 1–12)*. International Organization for Standardization, Geneva.
- [25] Kavitha, C., Rajendran, P., Saravanakumar, N. (2019). *Active camber and toe control strategy for the double wishbone suspension*. *Journal of King Saud University*, 31(4), 375–384. <https://doi.org/10.1016/j.jksues.2018.01.003>
- [26] Kimball, J. B., DeBoer, B., Bubbar, K. (2024). *Adaptive control and reinforcement learning for vehicle suspension control: A review*. *Annual Reviews in Control*, 58, 100974. <https://doi.org/10.1016/j.arcontrol.2024.100974>
- [27] Liu, M., Li, Y., Rong, X., Zhang, S., Yin, Y. (2020). *Semi-Active Suspension Control Based on Deep Reinforcement Learning*. *IEEE Access*, 8, 9978–9986. <https://doi.org/10.1109/ACCESS.2020.2964116>
- [28] Múčka, P. (2018). *Simulated Road Profiles According to ISO 8608 in Vibration Analysis*. *Journal of Testing and Evaluation*, 46(1), 20160265. <http://dx.doi.org/10.1520/JTE20160265>
- [29] Narvekar, S., Peng, B., Leonetti, M., Sinapov, J., Taylor, M. E., Stone, P. (2020). *Curriculum learning for reinforcement learning domains: A framework and survey*. *Journal of Machine Learning Research*, 21(181). <https://doi.org/10.48550/arXiv.2003.04960>
- [30] Ng, A. Y., Harada, D., Russell, S. (1999). *Policy invariance under reward transformations: Theory and application to reward shaping*. *Proceedings of the 16th International Conference on Machine Learning*, 278–287.
- [31] Nhu, A. N., Le, N.-A., Li, S., Truong, T. D. V. (2023). *Physics-Guided Reinforcement Learning for Realistic Vehicle Active Suspension Control*. *Proc. IEEE Int. Conf. on Machine Learning and Applications (ICMLA)*, 422–429. <https://doi.org/10.1109/ICMLA58977.2023.00065>
- [32] Paszke, A., Gross, S., Massa, F., et al. (2019). *PyTorch: An imperative style, high-performance deep learning library*. *Advances in Neural Information Processing Systems*, 32, 8024–8035. <https://doi.org/10.48550/arXiv.1912.01703>
- [33] Poussot-Vassal, C., Sename, O., Dugard, L. (2012). *Survey and performance evaluation on some automotive semi-active suspension control methods*. *Annual Reviews in Control*, 36(1), 148–160. <https://doi.org/10.1016/j.arcontrol.2012.03.011>

- [34] Tseng, H. E., Hrovat, D. (2015). *State of the art survey: active and semi-active suspension control*. *Vehicle System Dynamics*, 53(7), 1034–1062. <http://dx.doi.org/10.1080/00423114.2015.1037313>
- [35] Ultsch, J., Lechelt, J., Scheld, M., Sawodny, O. (2024). *Reinforcement Learning for Semi-Active Vertical Dynamics of a Ground Vehicle*. *Applied Sciences*, 14(14), 7066. <http://dx.doi.org/10.3390/app14167066>
- [36] Van Moffaert, K., Nowé, A. (2014). *Multi-objective reinforcement learning using sets of Pareto dominating policies*. *Journal of Machine Learning Research*, 15, 3663–3692.
- [37] Virtanen, P., Gommers, R., Oliphant, T. E., et al. (2020). *SciPy 1.0: fundamental algorithms for scientific computing in Python*. *Nature Methods*, 17(3), 261–272. <https://doi.org/10.1038/s41592-019-0686-2>
- [38] Wachi, A., Shen, X., Sui, Y. (2024). *A Survey of Constraint Formulations in Safe Reinforcement Learning*. *Proceedings of the 33rd International Joint Conference on Artificial Intelligence (IJCAI-24)*. <https://www.ijcai.org/proceedings/2024/0913.pdf>
- [39] Wang, Y., Xu, Z., Zhang, Y., Chen, Z. (2023). *Research on Deep Reinforcement Learning Control Algorithm for Active Suspension Considering Uncertain Time Delay*. *Sensors*, 23(18), 7827. <http://dx.doi.org/10.3390/s23187827>
- [40] Wang, C., Cui, X., Zhao, S., Zhou, X., Song, Y., Wang, Y., Guo, K. (2024). *A deep reinforcement learning-based active suspension control algorithm considering deterministic experience tracing for autonomous vehicles*. *Applied Soft Computing*, 153, 111259. <https://doi.org/10.1016/j.asoc.2024.111259>
- [41] Wen, Y. K. (1976). *Method for random vibration of hysteretic systems*. *Journal of the Engineering Mechanics Division (ASCE)*, 102(2), 249–263.
- [42] Zhu, C., et al. (2022). *Intelligent suspension control via curriculum RL*. *International Journal of Automotive Technology*, 23(5), 1123–1135. <http://dx.doi.org/10.1109/TIE.2010.2046581>

List of Symbols

Symbol	Description
z_s	Sprung mass displacement (m)
z_u	Unsprung mass displacement (m)
z_r	Road profile displacement (m)
\dot{z}_s	Sprung mass velocity (m/s)
\dot{z}_u	Unsprung mass velocity (m/s)
\ddot{z}_s	Sprung mass acceleration (m/s ²)
\ddot{z}_u	Unsprung mass acceleration (m/s ²)
F_a	Actuator force (N), control input
F_s	Suspension spring force (N)
F_f	Friction force (N)
F_t	Tire force (N)
m_s	Sprung mass (kg)
m_u	Unsprung mass (kg)
k_s	Suspension stiffness (N/m)
k_t	Tire stiffness (N/m)
c_s	Suspension damping coefficient (Ns/m)
λ_{load}	Load factor (dimensionless)
z_{limit}	Maximum allowable suspension travel (m)
r_t	Reward at time step t
q_{acc}	Penalty weight for body acceleration (comfort)
q_{travel}	Penalty weight for suspension travel (safety)
r_u	Penalty weight for actuator energy consumption
r_{du}	Penalty weight for control smoothness
$F_{a,\text{prev}}$	Actuator force at previous timestep (N)
$\mu_{\phi}(s)$	Actor network (deterministic policy)
$Q_{\theta_i}(s, a)$	Critic networks (action-value functions)
γ	Discount factor
τ	Soft target update rate
σ_b	Exploration noise std. deviation

σ_{targ}	Target policy smoothing noise
d_{π}	Policy update delay
\mathcal{D}	Replay buffer
E	Total number of episodes
T	Maximum number of steps per episode
$G_d(\Omega)$	Road roughness PSD
Ω	Spatial frequency (cycles/m)
RMS	Root-mean-square metric
ISO A–E	Road quality classes from very good (A) to very poor (E)

List of Figures

2.1	Quarter-car schematic with tire stiffness k_t , suspension stiffness k_s , damper c_s , and active actuator force F_a	6
2.2	Illustrative ISO 8608 road roughness PSD families (slope ≈ -2) across Classes A–E; Class E highlighted in green [28].	7
2.3	Taxonomy/evolution from passive to data-driven controllers (indicative, not exhaustive). Passive/semi-active/active adapted from [33]; classical robust control approaches from [34]; ML approaches such as fuzzy and neural networks from [6]; and DRL methods including TD3 from [17].	8
3.1	Enhanced quarter-car model schematic showing coordinate system, mass elements, and force-generating components.	14
3.2	Free body diagrams showing all forces acting on sprung and unsprung masses. Force directions are consistent with equations (3.25) and (3.26).	15
3.3	Progressive spring force-displacement characteristics showing linear region, cubic hardening, progressive spring effects, and bump-stop activation at ± 120 mm travel limits. Figure 3.3 demonstrates the progressive nature of the spring force characteristics. The linear region dominates for small deflections up to approximately 80mm, where the cubic hardening term $k_{nl}(z_s - z_u)^3$ becomes significant, providing a $3\times$ stiffness increase at the travel limits. The progressive spring term creates smooth stiffness transitions, while bump-stop forces activate sharply beyond ± 120 mm to prevent mechanical damage. This nonlinear behavior creates scenarios where adaptive control strategies can outperform linear controllers optimized for nominal operating points.	18
3.4	Hysteretic friction force characteristics showing stiction region ($ v < 0.001$ m/s) and sliding friction with viscous damping component.	20
3.5	ISO 8608 road roughness power spectral density functions for classes A through E, showing the characteristic Ω^{-2} slope.	24
3.6	Representative road profile examples for different ISO 8608 classes showing increasing roughness amplitude and frequency content.	26

3.7	Step response validation showing close agreement between theoretical linear model prediction and simulated nonlinear model behavior for small displacements.	29
3.8	Natural frequency validation results demonstrating model accuracy within accepted literature ranges for automotive suspension systems.	30
3.9	Nonlinearity analysis showing deflection regions where linear models become inadequate, justifying the need for adaptive control approaches.	30
3.10	Sensitivity of the quarter-car dynamics to physical parameter variations. The top row shows the effect of $\pm 20\%$ variation in sprung mass (left) and suspension stiffness (right) on the natural frequency. The bottom-left panel shows the influence of damping coefficient variation on the damping ratio. The bottom-right panel presents a Monte Carlo analysis with $\pm 10\%$ uncertainty in mass and stiffness, yielding a distribution of natural frequencies. The results indicate that the model predictions remain within realistic literature ranges, demonstrating robustness of the suspension dynamics to parameter uncertainty.	31
4.1	TD3-based active suspension control architecture with safety constraints. Solid arrows show control flow, dashed arrows show training data flow. The implementation does not employ a run-time predictive safety filter; instead, safety is enforced through action clipping/policy limits, smooth actuator saturation, and an adaptive demonstration schedule that temporarily increases LQR guidance if TD3 underperforms during training.	32
4.2	Episode return vs. environment steps. Curves show mean \pm one standard deviation over sliding windows.	44
5.1	Performance heatmaps showing RMS body acceleration across speed and road class combinations. Lower values (green) indicate better performance, while higher values (red) represent poorer vibration isolation.	54
5.2	Average performance across all road classes (left) and active control benefits relative to passive suspension (right). TD3 demonstrates consistent improvements with particular advantages at higher speeds. (Lower RMS Acc means better)	55
5.3	Three-dimensional performance surfaces showing the relationship between speed, road class, and RMS acceleration for each controller. The visualization clearly illustrates TD3's superior performance characteristics across the operational envelope.	56
5.4	RMS body acceleration distribution for Class A roads showing competitive performance between LQR and TD3 controllers on smooth surfaces.	57

5.5	RMS acceleration distributions for intermediate road classes showing the transition where TD3 begins to demonstrate advantages over traditional controllers.	58
5.6	RMS acceleration distributions for rough terrain showing substantial TD3 performance advantages where traditional controllers struggle with complex nonlinear dynamics.	59
5.7	Speed versus RMS acceleration curves for each road class, showing how controller performance varies with operating conditions. TD3 demonstrates increasing advantages as both speed and road roughness increase.	61
5.8	Actuator effort versus speed curves for each road class, showing energy consumption patterns. TD3 demonstrates efficient force utilization across all speed ranges compared to traditional controllers.	63
5.9	Mean absolute control force heatmaps illustrating energy consumption patterns. TD3 demonstrates efficient force utilization compared to traditional active controllers.	66
5.10	Control signal smoothness analysis across speeds showing RMS control rate, peak activity, and signal variability. TD3 demonstrates smoother control characteristics compared to traditional approaches.	68

List of Tables

2.1	Suspension types: qualitative comparison [33].	5
2.2	Evolution of suspension control methods and technology (indicative milestones).	7
2.3	Classical controllers: strengths vs. limitations [12, 33, 34].	9
2.4	Classical vs. DRL controllers: attribute-level comparison.	12
3.1	Baseline Physical Parameters	16
3.2	Parameter Justification and Literature Sources	16
3.3	Implemented Friction Model Parameters	19
3.4	ISO 8608 Road Classification (Implementation Values)	24
4.1	Implemented TD3 Hyperparameter Configuration	42
4.2	Safety rollbacks and constraint monitoring during training.	44
5.1	Complete Test Scenario Matrix	48
5.2	Simulation Configuration Parameters	52
5.3	Overall Performance Summary Across All Test Conditions	53
5.4	Maximum Suspension Travel Analysis Across All Test Scenarios	64
5.5	Maximum Mean Control Forces by Controller	65
5.6	TD3 vs. LQR RMS comparison by road class and speed (Welch's <i>t</i> -test). A downward arrow (↓) means TD3 has lower RMS (better).	70

List of Equations

2.1	Sprung mass equation of motion with active actuator force	6
2.2	Unsprung mass equation of motion including tire and actuator forces	6
3.1	Nonlinear suspension spring force with cubic hardening, progressive stiffening, and bump-stop	17
3.2	Cubic hardening coefficient for spring nonlinearity	17
3.3	Progressive spring constant for amplitude-dependent stiffening	17
3.4	Bump-stop force with piecewise quadratic characteristic	17
3.5	Suspension travel limit for bump-stop activation	17
3.6	Bump-stop stiffness parameter	17
3.7	First-order friction state dynamics with adaptation rate	18
3.8	Friction desired force model with stiction and sliding regimes	18
3.9	Breakaway friction force parameter for stiction regime	19
3.10	Coulomb friction force parameter for sliding regime	19
3.11	Viscous friction coefficient parameter	19
3.12	Stiction threshold velocity for friction regime transition	19
3.13	Effective damping with frequency and amplitude adaptation	20
3.14	Frequency adaptation factor for damping modulation	20
3.15	Amplitude adaptation factor for damping modulation	20
3.16	Frequency factor for high-frequency excitation capture	20
3.17	Amplitude factor for large suspension excursion response	21
3.18	Velocity-squared drag force for aerodynamic-like damping effects	21
3.19	Load-dependent sprung mass variation	21
3.20	Load-adaptive spring stiffness adjustment	21
3.21	Speed-dependent tire stiffness parameterization	21
3.22	Speed dependency gain for tire stiffness in SI units	21
3.23	State vector definition for quarter-car dynamics	22
3.24	Soft-clipping actuator saturation with smoothing parameter	22
3.25	Normalized actuator saturation ratio	22
3.26	Nonlinear tire force with polynomial stiffening characteristics	22

3.27	Tire damping force for high-frequency isolation	22
3.28	Effective damping force with adaptive characteristics	22
3.29	Actuator dynamics with first-order lag	23
3.30	Commanded force with smooth saturation characteristics	23
3.31	Maximum actuator force parameter	23
3.32	Saturation smoothing zone	23
3.33	Smoothing ratio for actuator saturation transition	23
3.34	ISO 8608 power spectral density function with frequency dependence . . .	24
3.35	Reference spatial frequency for ISO 8608 standard	24
3.36	Waviness parameter for road roughness characterization	24
3.37	Road profile as weighted sum of segment profiles	24
3.38	Total road length for simulation episodes	25
3.39	Spatial resolution for road discretization	25
3.40	Preview distance for predictive control	25
3.41	Number of preview points for road lookahead	25
3.42	Spectral synthesis of road profile from frequency components	25
3.43	Amplitude calculation from power spectral density	25
3.44	RMS body acceleration over evaluation horizon	27
3.45	Maximum suspension travel over evaluation horizon	27
3.46	RMS actuator force for energy consumption assessment	27
3.47	Maximum actuator force over evaluation horizon	27
3.48	Actuator saturation fraction over evaluation period	27
3.49	Control smoothness metric for actuator force derivatives	27
3.50	Composite performance index with normalized multi-objective metrics . .	27
3.51	Runge-Kutta 4th order first stage derivative	28
3.52	Runge-Kutta 4th order second stage derivative	28
3.53	Runge-Kutta 4th order third stage derivative	28
3.54	Runge-Kutta 4th order fourth stage derivative	28
3.55	Runge-Kutta 4th order state vector update formula	28
4.1	Observation vector with state variables, road preview, and system features	33
4.2	Action space definition for commanded actuator force	34
4.3	Suspension travel constraint for physical safety	34
4.4	Actuator force constraint for hardware protection	34
4.5	Multi-objective reward function with load-adaptive penalties	34
4.6	Load-adaptive comfort penalty weight	34

4.7	Load-adaptive safety penalty weight	35
4.8	Energy consumption penalty weight	35
4.9	Control smoothness penalty weight	35
4.10	Keep-out bonus for operating within safe travel limits	35
4.11	Adaptation bonus for smooth acceleration under load variation	35
4.12	Friction penalty for energy-efficient operation	35
4.13	Actor network first hidden layer with ReLU activation	36
4.14	Actor network second hidden layer with ReLU activation	36
4.15	Actor network third hidden layer with ReLU activation	36
4.16	Actor network output layer with tanh activation and force scaling	36
4.17	Critic network concatenated state-action input vector	36
4.18	Twin critic networks first hidden layer with ReLU activation	36
4.19	Twin critic networks second hidden layer with ReLU activation	36
4.20	Twin critic networks third hidden layer with ReLU activation	36
4.21	Twin critic Q-value outputs for TD3 algorithm	36
4.22	TD3+BC actor loss with behavioral cloning regularization	38
4.23	Behavioral cloning weight decay schedule for online fine-tuning	38
4.24	Demonstration mixing probability with speed and episode adaptation	39
4.25	Base mixing probability with visit count decay	39
4.26	Adaptive demonstration floor parameter	39
4.27	Speed-dependent boost factors for challenging scenarios	39
4.28	Rollback safety mechanism trigger condition	39
4.29	Episode-dependent rollback threshold schedule	40
4.30	Multi-stage curriculum learning speed progression schedule	40
4.31	Inverse frequency weighting for speed selection	40
4.32	Discrete load factor values for systematic evaluation	41
4.33	Push-window actor learning rate	41
4.34	Push-window critic learning rate	41
4.35	Demonstration floor target during push window	41
4.36	Cosine annealing learning rate schedule	43
4.37	Exponential exploration noise decay schedule	43
5.1	LQR cost function for optimal control design	49
5.2	State weighting matrix Q for LQR controller	50
5.3	Control input weighting scalar R for LQR controller	50
5.4	PID control law with proportional, integral, and derivative terms	50

5.5	Proportional gain for PID controller	50
5.6	Integral gain for PID controller	50
5.7	Derivative gain for PID controller	50
5.8	RMS body acceleration metric for vibration isolation assessment	51
5.9	Maximum suspension travel metric for constraint monitoring	51
5.10	Actuator saturation fraction over evaluation period	51
5.11	Mean absolute actuator force for energy assessment	52
5.12	TD3 relative improvement efficiency over LQR baseline	70
5.13	Episode return normalized by traveled distance for speed-independent comparison	70